

1 ***Drosophila* models of pathogenic copy-number variant genes show global and**
2 **non-neuronal defects during development**

3

4 Tanzeen Yusuff^{1,4}, Matthew Jensen^{1,4}, Sneha Yennawar^{1,4}, Lucilla Pizzo¹, Siddharth
5 Karthikeyan¹, Dagny J. Gould¹, Avik Sarker¹, Yurika Matsui^{1,2}, Janani Iyer¹, Zhi-Chun Lai^{1,2},
6 and Santhosh Girirajan^{1,3*}

7

8 1. Department of Biochemistry and Molecular Biology, Pennsylvania State University,
9 University Park, PA 16802

10 2. Department of Biology, Pennsylvania State University, University Park, PA 16802

11 3. Department of Anthropology, Pennsylvania State University, University Park, PA 16802

12

13 ⁴ contributed equally to work

14

15

16 *Correspondence:

17 Santhosh Girirajan, MBBS, PhD

18 205A Life Sciences Building

19 Pennsylvania State University

20 University Park, PA 16802

21 E-mail: sxg47@psu.edu

22 Phone: 814-865-0674

23

24 **ABSTRACT**

25 While rare pathogenic CNVs are associated with both neuronal and non-neuronal phenotypes,
26 functional studies evaluating these regions have focused on the molecular basis of neuronal
27 defects. We report a systematic functional analysis of non-neuronal phenotypes for 59 homologs
28 of genes within ten CNVs and 20 neurodevelopmental genes in *Drosophila*. Using wing-specific
29 knockdown of 136 RNA interference lines, we identify phenotypes in 72/79 homologs including
30 six lines with lethality and 21 lines with severe phenotypes. We find no correlation between
31 severity of these phenotypes and neuronal defects due to eye-specific knockdown. We observe
32 disruptions in cell proliferation and apoptosis for 23/27 homologs, and altered Wnt, Hedgehog
33 and Notch signaling for 9/14 homologs, including *AATF/Aatf*, *PPP4C/Pp4-19C*, and
34 *KIF11/Klp61F*, validated with differences in human tissue-specific expression and network
35 connectivity. Our findings suggest that multiple genes within each CNV differentially affect both
36 global and tissue-specific developmental processes, contributing to non-neuronal phenotypes of
37 CNV disorders.

38

39

40 INTRODUCTION

41 Rare copy-number variants (CNVs), or deletions and duplications in the genome, are associated
42 with neurodevelopmental disorders such as autism, intellectual disability (ID), and
43 schizophrenia^{1,2}. While dosage alteration of CNV regions contribute predominantly to defects in
44 nervous system development, several CNV disorders also lead to early developmental features
45 involving other organ systems^{3,4}, including cardiac defects^{5,6}, kidney malformations⁷,
46 craniofacial features³, and skeletal abnormalities⁸. In fact, an overall survey of ten rare disease-
47 associated CNVs among individuals within the DECIPHER database⁹ showed a wide range of
48 non-neuronal phenotypes across multiple organ systems for each CNV disorder (**Fig. 1**). For
49 example, the 1q21.1 deletion causes variable expression of multiple neuronal and non-neuronal
50 phenotypes, including developmental delay, autism, and schizophrenia as well as craniofacial
51 features, cataracts, cardiac defects, and skeletal abnormalities¹⁰⁻¹². Additionally, while the
52 7q11.23 deletion associated with Williams-Beuren syndrome (WBS) causes neuropsychiatric and
53 behavioral features, other non-neuronal phenotypes, including supravalvular aortic stenosis,
54 auditory defects, hypertension, diabetes mellitus, and musculoskeletal and connective tissue
55 anomalies, are also observed among the deletion carriers¹³. In fact, individual genes within the
56 WBS region are associated with specific features of the deletion, such as *ELN* and supravalvular
57 aortic stenosis¹⁴, *STX1A* and impaired glucose tolerance¹⁵, *LIMK1* and impaired visuospatial
58 abilities¹⁶, and *GTF2IRD1* and craniofacial abnormalities¹⁷. Furthermore, *TBX1* was identified to
59 cause the pharyngeal arch cardiac defects associated with the 22q11.2 deletion (DiGeorge
60 syndrome)¹⁸, while *HNF1B* within the 17q12 deletion region was identified as the causative gene
61 for kidney defects associated with the deletion^{19,20}. However, candidate genes for a majority of
62 non-neuronal phenotypes have not been identified for several rare CNV disorders, in particular

63 for CNVs associated with variably-expressive phenotypes such as the 1q21.1 deletion and the
64 16p11.2 deletion^{21,22}. Additionally, affected individuals who carry disruptive mutations in
65 neurodevelopmental genes from recent sequencing studies have also been documented to
66 manifest non-neuronal phenotypes. For example, individuals with loss-of-function mutations in
67 the autism-associated gene *CHD8* present with gastrointestinal problems, tall stature, and
68 craniofacial features in addition to neuropsychiatric features²³, while mutations in the
69 microcephaly-associated gene *KIF11* also lead to congenital lymphedema and retinopathy²⁴.

70 Despite the importance of identifying genes within CNVs that contribute towards non-
71 neuronal phenotypes, functional studies of CNV genes have primarily focused on detailed
72 assessments of neuronal phenotypes in model systems. For example, mouse models generated for
73 the 16p11.2 deletion exhibited post-natal lethality, reduced brain size and neural progenitor cell
74 count, motor and habituation defects, synaptic defects, and behavioral defects²⁵⁻²⁷. Similarly,
75 mouse models for the 3q29 deletion showed decreased weight and brain size, increased
76 locomotor activity and startle response, and decreased spatial learning and memory^{28,29}.
77 However, fewer studies have focused on detailed evaluation of non-neuronal phenotypes in
78 functional models of CNV disorders. For example, Arbogast and colleagues evaluated obesity
79 and metabolic changes in 16p11.2 deletion mice, which showed reduced weight and impaired
80 adipogenesis³⁰. While Haller and colleagues showed that mice with knockdown of *MAZ*, a gene
81 within the 16p11.2 deletion region, contribute to the genitourinary defects observed in
82 individuals with the deletion³¹, mouse studies on other homologs of 16p11.2 genes, including
83 *TAOK2*, *KCTD13*, and *MAPK3*, have only focused on assessing neuronal defects³²⁻³⁶.
84 Furthermore, Dickinson and colleagues reported a high-throughput analysis of essential genes in
85 mice and identified both neuronal and non-neuronal phenotypes for individual gene knockouts,

86 including more than 400 genes that lead to lethality³⁷. While these efforts aided in implicating
87 novel genes with human disease, our understanding of how genes associated with
88 neurodevelopmental disorders contribute towards non-neuronal phenotypes is still limited.
89 Therefore, a large-scale analysis of non-neuronal phenotypes is necessary to identify specific
90 candidate genes within CNV regions and associated biological mechanisms that contribute
91 towards these phenotypes.

92 *Drosophila melanogaster* is an excellent model system to evaluate homologs of
93 neurodevelopmental genes, as many developmental processes and signaling pathways are
94 conserved between humans and flies³⁸. In fact, over 75% of human disease genes have homologs
95 in *Drosophila*, including many genes involved in cellular signaling processes^{39,40}. We recently
96 examined the contributions of individual *Drosophila* homologs of 28 genes within the 16p11.2
97 and 3q29 deletion regions towards specific neurodevelopmental phenotypes, including rough eye
98 phenotypes and defects in climbing ability, axon targeting, neuromuscular junction, and dendritic
99 arborization^{41,42}. While these findings implicated multiple genes within each CNV region
100 towards neuronal phenotypes, the conserved role of these genes towards non-neuronal
101 phenotypes is not well understood. The *Drosophila* wing is an effective model system to
102 evaluate such developmental phenotypes, as key components of conserved signaling pathways,
103 such as Notch, epidermal growth factor receptor (EGFR), Hedgehog, and Wnt pathways, were
104 identified using fly wing models⁴³⁻⁴⁹. For example, Wu and colleagues showed that
105 overexpression of the *Drosophila* homolog for *UBE3A*, associated with Angelman syndrome,
106 leads to abnormal wing and eye morphology defects⁵⁰. Furthermore, *Drosophila* mutant screens
107 for developmental phenotypes, including wing defects, were used to identify conserved genes for
108 several human genetic diseases, including Charcot-Marie-Tooth disease and syndromic

109 microcephaly⁵¹. Kochinke and colleagues also recently performed a large-scale screening of ID-
110 associated genes, and found an enrichment of wing trichome density and missing vein
111 phenotypes in ID genes compared to control gene sets⁵². Hence, the fly wing provides a model
112 system that is ideal for evaluating the contributions of individual homologs of CNV genes
113 towards cellular and developmental phenotypes.

114 In this study, we tested the non-neuronal phenotypes of 79 fly homologs of human genes
115 within ten pathogenic CNV regions and genes associated with neurodevelopmental disorders.
116 We observed a wide range of robust qualitative and quantitative adult wing phenotypes among
117 the 136 RNA interference (RNAi) lines tested in our study, including size defects, ectopic and
118 missing veins, severe wrinkling, and lethality. Further analysis of cellular phenotypes revealed
119 disruptions in conserved developmental processes in the larval imaginal wing disc, including
120 altered levels of cell proliferation and apoptosis as well as altered expression patterns in the Wnt,
121 Hedgehog, and Notch signaling pathways. However, we found no correlation in the severity of
122 phenotypes observed with wing and eye-specific knockdown. Our findings were further
123 supported by differences in expression patterns and network connectivity of human CNV genes
124 across different tissues. Our analysis emphasizes the importance of multiple genes within each
125 CNV region towards both global and tissue-specific developmental processes, potentially
126 accounting for the non-neuronal phenotypes associated with pathogenic CNVs.

127

128 RESULTS

129 Wing-specific knockdown of fly homologs of CNV genes show non-neuronal phenotypes

130 Using an RNAi based analysis driven by the *bx^{MS1096}-GAL4* wing-specific driver, we tested a
131 total of 136 RNAi lines for 59 homologs of genes within pathogenic CNV regions (chromosomal
132 locations 1q21.1, 3q29, 7q11.23, 15q11.2, 15q13.3, 16p11.2, distal 16p11.2, 16p12.1, 16p13.11,
133 and 17q12) and 20 homologs of genes associated with neurodevelopmental disorders (**Supp.**
134 **Data 1**). Fly homologs of these genes were identified using the DIOPT orthology prediction
135 tool⁵³. We list both the human gene name and the fly gene name for each tested gene as *HUMAN*
136 *GENE/Fly gene* (i.e. *KCTD13/CG10465*) as well as the human CNV region for context at first
137 instance. We scored 20-25 adult wings for five distinct wing phenotypes in each non-lethal
138 RNAi line, including wrinkled wing, discoloration, ectopic veins, missing veins, and bristle
139 planar polarity phenotypes (**Fig. 2A; Supp. Data 2**). We first categorized each wing phenotype
140 based on their severity and performed k-means clustering analysis to categorize each RNAi line
141 by their overall phenotype severity (**Fig. 2B-C**). We observed four clusters of RNAi lines: 75
142 lines with no observable qualitative phenotypes (55.2%), 24 lines with mild phenotypes (17.7%),
143 10 lines with moderate phenotypes (7.4%), 21 lines with severe phenotypes (15.4%), and 6 lines
144 with lethal phenotypes (4.4%), including *ACACA/ACC* within 17q12, *DLG1/dlg1* within 3q29,
145 and *STX1A/Syx1A* within 7q11.23 (**Fig. 2B-D; Supp. Data 2**). We observed severe wrinkled
146 wing phenotypes for 13/79 fly homologs, including *PPP4C/Pp4-19C* within 16p11.2,
147 *ATXN2L/Atx2* within distal 16p11.2, *AATF/Aatf* within 17q12, and *MFI2/Tsf2* within 3q29 (**Fig.**
148 **3A-B, Supp. Data 3**). Interestingly, seven out of ten CNV regions contained at least one
149 homolog that showed lethality or severe wing phenotypes, and five CNV regions (3q29, 16p11.2,
150 distal 16p11.2, 16p12.1, and 17q12) had multiple homologs showing lethality or severe wing

151 phenotypes (**Fig. 3A, Supp. Data 3**). For example, RNAi lines for both *UQCRC2/UQCR-C2* and
152 *POLR3E/Sin* within 16p12.1 showed lethality. Within the 3q29 region, *NCBP2/Cbp20* and
153 *MFI2/Tsf2* showed severe phenotypes while *DLG1/dlg1* showed lethality. In contrast, 12/20
154 known neurodevelopmental genes showed no observable wing phenotypes, suggesting that these
155 genes could be responsible for neuronal-specific phenotypes (**Fig. 3B, Supp. Data 3**). We note
156 that 18/79 fly homologs showed discordant phenotypes between two or more RNAi lines for the
157 same gene, which could be due to differences in expression of the RNAi construct among these
158 lines (**Supp. Data 3**).

159 Certain qualitative phenotypes exhibited higher frequency in males compared to females.
160 For example, discoloration (87 lines in males compared to 56 lines in females; $p=1.315\times 10^{-4}$,
161 two-tailed Fisher's exact test) and missing vein phenotypes (92 lines in males compared to 29
162 lines in females; $p=2.848\times 10^{-16}$, two-tailed Fisher's exact test) at any degree of severity were
163 more commonly observed in males than females (**Supp. Data 2**). In particular, 25/92 lines in
164 males (compared to 1/29 in females) showed a total loss of the anterior crossvein (ACV) (**Supp.**
165 **Data 2**). We further identified 17 RNAi lines that were lethal in males with wing-specific
166 knockdown of fly homologs. While higher frequencies of wing phenotypes in males could be
167 due to a sex-specific bias of developmental phenotypes, the increased severity we observed in
168 males is most likely due to a stronger RNAi knockdown caused by an X-linked dosage
169 compensation, as the *bx^{MS1096}-GAL4* driver is inserted on the fly X chromosome^{54,55}.

170 Next, we measured the total adult wing area and the lengths of six veins (longitudinal L2,
171 L3, L4, L5, ACV, and posterior crossvein or PCV) in the adult wing for each of the tested RNAi
172 lines that did not show lethality (or severe wrinkled phenotypes for vein length measurements)
173 (**Fig. 4A**). Overall, we identified significant wing measurement changes for 89 RNAi lines

174 compared to controls, which included lines that did not have an observable qualitative wing
175 phenotype (**Fig. 2D**). A summary of L3 vein lengths is presented in **Fig. 4B**, and the
176 measurements for the remaining five veins are presented in **Supp. Figure 1** and **Supp. Data. 2**.
177 We found that 33/61 of the homologs (54%) showed significant changes in L3 vein length,
178 including 20 homologs with longer vein lengths and 13 homologs with shorter vein lengths
179 (**Supp. Data 3**). Additionally, 41/74 of the fly homologs (55%) showed changes in wing area
180 (**Supp. Data 3**), including 36 homologs which showed smaller wing areas and five homologs
181 showed larger wing areas compared to controls (**Supp. Data 3**). For example, both homologs of
182 genes within 1q21.1 region, *BCL9/lgs* and *FMO5/Fmo-2*, showed decreased wing area and vein
183 length, potentially mirroring the reduced body length phenotype observed in mouse models of
184 the deletion⁵⁶ (**Fig. 4B-C**). In addition, *PAK2/Pak* within 3q29, *TBX1/org-1* within 22q11.2,
185 autism-associated *CHD8/kis*, and microcephaly-associated *ASPM/asp* also showed smaller wing
186 areas and vein lengths (**Fig. 4B-C**). In contrast, *TRPM1/Trpm* within 15q13.3 and the cell
187 proliferation gene *PTEN/Pten*⁵⁷ both showed larger wing areas and vein lengths (**Fig. 4B-C**).
188 Furthermore, we identified eight homologs that showed no qualitative wing phenotypes but had
189 significant changes in wing areas and vein lengths (**Supp. Data 3**), including *CCDC101/Sgf29* in
190 distal 16p11.2, *FMO5/Fmo-2*, *TRPM1/Trpm*, *DHRS11/CG9150* in 17q12, and *NSUN5/Nsun5* in
191 7q11.23 (**Fig. 4B-C; Supp. Data 3**). These results indicate that homologs of certain CNV genes
192 may influence variations in size without causing adverse wing phenotypes, and may be
193 specifically implicated towards cellular growth mechanisms.

194

195

196

197 **Homologs of CNV genes show global and tissue-specific effects during development**

198 We previously showed that many of the same fly homologs of CNV genes that showed wing
199 defects in the current study also contributed towards neuronal phenotypes in the fly eye^{41,42},
200 suggesting a role for these genes in global development. We therefore performed ubiquitous and
201 eye-specific knockdown of fly homologs to assess tissue-specific effects in comparison to the
202 wing phenotypes. First, we used the *da-GAL4* driver at 25°C to drive ubiquitous knockdown of
203 RNAi lines for 31 homologs of CNV genes, including 19 that were previously published^{41,42}, and
204 observed complete or partial lethality at larval and pupal stages with knockdown of 10/31
205 homologs (32.3%) (**Fig. 5A**). Lethal phenotypes have also been documented for 43/130
206 knockout mouse models of individual CNV genes as well as for the entire deletion (**Supp. Data**
207 **4**). For example, mouse models heterozygous for the 16p11.2 deletion showed partial neonatal
208 lethality, while knockout mouse models of four individual genes within the 16p11.2 region,
209 including *Ppp4C*^{-/-} and *Kif22*^{-/-}, showed embryonic lethality^{25,58,59}. In our study, the *DLG1/dlg1*
210 line that showed lethality with wing-specific knockdown also exhibited larval lethality with
211 ubiquitous knockdown, indicating its role in global development (**Fig. 5A**). In addition, six
212 homologs that showed severe wing phenotypes also showed larval or pupal lethality with
213 ubiquitous knockdown, including *ALDOA/Ald* and *PPP4C/Pp4-19C* within 16p11.2 and
214 *ATXN2L/Atx2* and *TUFM/mEFTu1* within distal 16p11.2 (**Fig. 5A**). The remaining homologs
215 that showed lethality with ubiquitous knockdown showed at least a mild qualitative or
216 quantitative wing phenotype.

217 We next compared the phenotypes observed with wing-specific knockdown of fly
218 homologs to their corresponding eye-specific knockdowns to evaluate neuronal versus non-
219 neuronal effects. To quantitatively assess the phenotypic severity of cellular defects with eye-

220 specific knockdown of fly homologs, we developed a tool called *Flynotyper*⁶⁰ that determines the
221 degree of disorganization among the ommatidia in the adult eye. We analyzed phenotypic scores
222 obtained from *Flynotyper* for 66 RNAi lines of 45 fly homologs, including from previously-
223 published datasets^{41,42,60}. We found that 37/45 homologs (82.2%) exhibited both eye and wing-
224 specific defects (**Fig. 5B, Supp. Fig. 2, Supp. Data 5**). Two homologs with significant eye
225 phenotypes did not show any wing phenotypes, including *SPNS1/spin* within distal 16p11.2 and
226 microcephaly-associated *SLC25A19/Tpc1*⁶¹, while five homologs only showed wing-specific
227 phenotypes, including *CDIPT/Pis* and *YPEL3/CG15309* within 16p11.2, *FBXO45/Fsn* and
228 *OSTalpha/CG6836* within 3q29, and *UQCRC2/UQCR-C2* (**Fig. 5B, Supp. Fig. 2**). In particular,
229 *UQCRC2/UQCR-C2* showed lethality with wing-specific knockdown, suggesting potential
230 tissue-specific effects of this gene in non-neuronal cells (**Fig. 5B**). While most homologs
231 contributed towards both eye and wing-specific phenotypes, we observed a wide range of
232 severity in eye phenotypes that did not correlate with the severity of quantitative or qualitative
233 wing phenotypes (**Fig. 5C**). For example, *TUFM/mEFTu1* showed a severe wing phenotype but
234 only a mild increase in eye phenotypic score, while *SH2B1/Lnk*, also within the distal 16p11.2
235 region, showed severe rough eye phenotypes but only a mild increase in wing size (**Fig. 5D**).
236 Similarly, *BCL9/lgs* also showed opposing tissue-specific effects with mild qualitative wing
237 phenotype and severe eye phenotype, suggesting that the role of these homologs towards
238 development differs across tissue types.

239

240 **CNV genes show variable expression across different tissues in flies and humans**

241 To assess how expression levels of CNV genes vary across different tissues, we first examined
242 the expression patterns of fly homologs in larval and adult tissues using the FlyAtlas Anatomical

243 Microarray dataset⁶². We found that 76/77 homologs with available data were expressed in at
244 least one larval and adult tissue (**Supp. Fig. 3, Supp. Data 6**). In general, we did not observe a
245 correlation between wing phenotype severity and expression patterns of homologs in larval or
246 adult tissues (**Fig. 6A**). For example, 58/77 homologs (75.3%) showed ubiquitous larval
247 expression, including both fly homologs that showed no qualitative wing phenotypes, such as
248 *KCTD13/CG10465* within 16p11.2 and *FBXO45/Fsn*, and those with severe wing phenotypes,
249 such as *PPP4C/Pp4-19C* and *NCBP2/Cbp20* (**Fig. 6A, Supp. Fig. 3**). Furthermore, 30/39
250 homologs (76.9%) that showed eye phenotypes also had ubiquitous larval expression, providing
251 further support to the observation that genes causing neuronal phenotypes may also contribute to
252 developmental phenotypes in other tissues (**Supp. Data 5**). Of note, 9/77 homologs (11.7%) did
253 not have any expression in the larval central nervous system, including *FMO5/Fmo-2*,
254 *BDHI/CG8888* within 3q29, and *TBX6/Doc2* within 16p11.2 (**Fig. 6A, Supp. Fig. 3**). However,
255 we observed wing phenotypes for 8/9 of these homologs, suggesting that they may contribute to
256 tissue-specific phenotypes outside of the nervous system. Except for the epilepsy-associated
257 *SCN1A/para*⁶³, which was exclusively expressed in both the larval central nervous system (CNS)
258 and adult brain tissues, other tested neurodevelopmental genes were also expressed in non-
259 neuronal tissues (**Fig. 6A**).

260 We further used the GTEx Consortium dataset⁶⁴ to examine tissue-specific expression of
261 150 human CNV and known neurodevelopmental genes across six tissues including brain, heart,
262 kidney, lung, liver, and muscle. We found 121 genes that were expressed in at least one adult
263 tissue, including 49 genes (32.7%) that showed ubiquitous expression across all six tissues
264 (**Supp. Data 6**). Of the 112 genes expressed in non-neuronal tissues, 34 did not have any
265 neuronal expression, including *TBX1*, *FMO5* and *GJA5* within 1q21.1, and *ATP2A1* within distal

266 16p11.2 (**Fig. 6B, Supp. Data 6**). *FMO5* and *TBX1* also showed non-neuronal expression in
267 *Drosophila* tissues, suggesting that their tissue-specific expression is highly conserved (**Fig. 6A**).
268 Other genes showing ubiquitous expression also had preferentially high expression for specific
269 non-neuronal tissues, including *ALDOA* and *UQCRC2* for muscle and heart for (**Fig. 6B**). In
270 contrast, we found nine genes that were expressed only in the adult brain, including *FAM57B*
271 and *DOC2A* within 16p11.2, as well as *SCN1A*, which showed similar CNS-only expression in
272 *Drosophila* tissues (**Fig. 6B, Supp. Data 6**).

273

274 **Knockdown of fly homologs of CNV genes lead to disruption of basic cellular processes**

275 The disruption of basic cellular processes in neuronal cells, such as cell proliferation and
276 apoptosis, have been implicated in neurodevelopmental disorders⁶⁵⁻⁶⁷. We previously identified
277 defects in cell proliferation among photoreceptors neurons in larval eye discs with knockdown of
278 16p11.2 homologs, as well as increased apoptosis with knockdown of a subset of 3q29
279 homologs^{41,42}. Here, we explored how these basic cellular processes are altered in non-neuronal
280 cells, specifically in the developing wing disc. We targeted 27 fly homologs that showed a range
281 of adult wing phenotypes for changes in cell proliferation and apoptosis, using anti-phospho-
282 Histone H3 Ser10 (pH3) and anti-*Drosophila* caspase-1 (*dcp1*), respectively, in the third instar
283 larval wing discs. We identified 23/27 homologs that showed significant increases in apoptotic
284 cells compared to controls, including seven homologs, such as *PPP4C/Pp4-19C*, *ATXN2L/Atx2*,
285 and *AATF/Aatf*, which showed *dcp1* staining across the entire larval wing pouch (**Fig. 7A-B,**
286 **Supp. Figs. 4-5, Supp. Data 7**). In addition, 16/27 genes showed decreased levels of
287 proliferation, including eight homologs which also showed apoptosis defects, such as
288 *CYFIP1/Sra-1* within 15q11.2, *SH2B1/Lnk*, and the microcephaly gene *KIF11/Klp61F* (**Fig. 7A**

289 **and 7C, Supp. Figs. 4-5, Supp. Data 7).** All six of the tested homologs with severe adult wing
290 phenotypes showed both increased apoptosis and decreased proliferation (**Supp. Data 7**).
291 Similarly, 3/4 homologs of genes showing lethality with wing-specific knockdown also showed
292 defects in apoptosis or proliferation, with the exception of *ACACA/ACC* (**Supp. Figure 4, Supp.**
293 **Data 7**). As *bx^{MS1096}-GAL4* is located on the X-chromosome, we expected to see more severe
294 defects in males compared with females with knockdown of homologs due to the X-linked
295 dosage compensation^{54,55}. However, knockdown of 3/11 tested homologs with sex-specific
296 differences in adult wing phenotypes, including *BCL9/lgs*, *CYFIP1/Sra-1*, and
297 *DNAJC30/CG11035* within 7q11.23, showed significantly decreased levels of cell proliferation
298 in females but no change for males compared to their respective controls, suggesting a sex-
299 specific effect of these genes for cell proliferation (**Supp. Fig. 5, Supp. Data 7**). Overall, our
300 results suggest that cell proliferation and apoptosis play an important role towards development
301 in both neuronal and non-neuronal tissues.

302

303 **Homologs of candidate CNV genes disrupt conserved signaling pathways**

304 Several conserved signaling pathways that are active in a spatial and temporal manner in the
305 larval wing disc, such as Wnt, Hedgehog, BMP, and Notch signaling, regulate the anterior-
306 posterior (A/P) and dorsal-ventral (D/V) boundaries to determine accurate morphology and vein
307 patterning in the adult wing^{48,49,68-70}. For example, Wnt and Notch signaling pathways both act
308 along the D/V boundary to determine cell fate^{71,72}, while Hedgehog signaling is dependent upon
309 expression of both engrailed in the posterior compartment and patched along the A/P border^{73,74}.
310 Furthermore, O’Roak and colleagues showed that genes identified from *de novo* mutations in
311 patients with autism are linked to β -catenin/Wnt pathway⁷⁵. In addition, familial loss-of-function

312 mutations in the human hedgehog signaling pathway gene *PTCH1* are implicated in basal cell
313 nevus syndrome, leading to basal cell carcinoma^{76,77}.

314 Based on adult wing phenotypes and disruptions to cellular processes, we next tested
315 whether knockdown of 14 fly homologs disrupt conserved signaling pathways in the third instar
316 larval wing disc (**Supp. Data 7**). In particular, we evaluated the role of Wnt, Hedgehog, and
317 Notch signaling pathways by testing the expression patterns of four key proteins within these
318 pathways, including wingless (Wnt), patched (Hedgehog), engrailed (Hedgehog), and delta
319 (Notch). We found that 9/14 homologs, including 8/10 homologs showing severe wing
320 phenotypes or lethality, exhibited disruptions in at least one signaling pathway. For example, five
321 homologs with severe or lethal phenotypes showed disruptions of all four signaling pathways,
322 including *AATF/Aatf*, *NCBP2/Cbp20*, *POLR3E/Sin*, *PPP4C/Pp4-19C*, and *KIF11/Klp61F* (**Fig.**
323 **8, Supp. Data 7**). Our observations are in concordance with previous findings by Swarup and
324 colleagues, who showed that *PPP4C/Pp4-19C* is a candidate regulator of Wnt and Notch
325 signaling pathways in *Drosophila* larval wing discs⁷⁸. Furthermore, two genes from the 3q29
326 region, *DLG1/dlg1* and *MFI2/Tsf2*, showed altered expression patterns for delta and patched but
327 not for engrailed, indicating that they selectively interact with the Hedgehog as well as Notch
328 signaling pathway (**Supp. Fig. 6**). In fact, Six and colleagues showed that Dlg1 directly binds to
329 the PDZ-binding domain of Delta⁷⁹. In contrast, *ACACA/ACC* and *UQCRC2/UQCR-C2* showed
330 no changes in expression patterns for any of the four signaling proteins tested, suggesting that the
331 observed lethality could be due to other cellular mechanisms (**Supp. Fig. 6**). We conclude that a
332 subset of homologs disrupt the expression of key proteins in signaling pathways, potentially
333 accounting for the developmental phenotypes observed in the adult wings.

334

335 **Connectivity patterns of candidate genes vary across human tissue-specific networks**

336 We examined patterns of connectivity for the nine candidate genes which showed disruptions of
337 signaling pathways within the context of human brain, heart, and kidney-specific gene
338 interaction networks⁸⁰. These tissue-specific networks were constructed using Bayesian
339 classifier-generated probabilities for pairwise genetic interactions based on co-expression data⁸⁰.
340 We calculated the lengths of the shortest paths between each candidate gene and 267 Wnt,
341 Notch, and Hedgehog pathway genes in each network as a proxy for connectivity (**Supp. Data**
342 **8**). In all three networks, each of the candidate genes were connected to a majority of the tested
343 signaling pathway genes, suggesting that our results have translational relevance towards human
344 developmental pathways (**Fig. 9A, Supp. Fig. 7**). Interestingly, we observed a higher
345 connectivity (i.e. shorter path distances) between candidate genes and Wnt and Hedgehog
346 pathway genes in the brain-specific network compared to the heart and kidney-specific networks
347 (**Fig. 9B**). We further identified enrichments for genes involved in specific biological processes
348 among the connector genes that were located in the shortest paths within neuronal and non-
349 neuronal tissue-specific networks (**Fig. 9C, Supp. Data 8**). For example, axon-dendrite
350 transport, dopaminergic signaling, and signal transduction functions were enriched among
351 connector genes only for the brain-specific network, while organelle organization and protein
352 ubiquitination were enriched among connector genes only for kidney and heart networks (**Fig.**
353 **9C**). However, several core biological processes, such as cell cycle, protein metabolism,
354 transcriptional regulation, and RNA processing/splicing, were enriched among connector genes
355 within all three tissue-specific networks (**Fig. 9C**). Our analysis highlights that human CNV
356 genes potentially interact with developmental signaling pathways in an ubiquitous manner, but
357 may affect different biological processes in neuronal and non-neuronal tissues.

358 **DISCUSSION**

359 We used the *Drosophila* wing as a model to identify key CNV genes involved in non-neuronal
360 phenotypes associated with CNV disorders. We tested fly homologs of 79 genes and identified
361 multiple homologs within each CNV region that exhibited strong phenotypes indicative of
362 developmental disruptions. Several themes have emerged from our study highlighting the
363 importance of fly homologs of CNV genes towards both global and tissue-specific phenotypes
364 associated with human CNV disorders.

365 *First*, we found that homologs of CNV genes contribute towards developmental
366 phenotypes through ubiquitous roles in neuronal and non-neuronal tissues. Although we did not
367 study models for the entire CNV, nearly all individual fly homologs of CNV genes contribute to
368 wing-specific developmental phenotypes. It is likely that these genes may also contribute to
369 additional phenotypes in other tissues that we did not assess. In fact, a subset of these genes also
370 showed early lethality with ubiquitous knockdown in addition to severe or lethal wing-specific
371 phenotypes. However, we found no correlation between the severity of the eye and wing
372 phenotypes, suggesting tissue-specific effects of these homologs towards developmental
373 phenotypes. In contrast, fly homologs of known neurodevelopmental genes generally showed
374 milder wing phenotypes compared with eye phenotypes, indicating a more neuronal role for
375 these genes. While our study only examined a subset of CNV genes with *Drosophila* homologs,
376 phenotypic data from knockout mouse models also support a global developmental role for
377 individual CNV genes. In fact, 44/130 knockout models of CNV genes within the Mouse
378 Genome Informatics (MGI) database⁸¹ exhibited non-neuronal phenotypes, including 20
379 homologs of CNV genes that showed both neuronal and non-neuronal phenotypes (**Supp. Data**
380 **4**). For example, knockout mouse models of *Dlg1*^{-/-} show defects in dendritic growth and

381 branching in the developing nervous system, in addition to craniofacial features and multiple
382 kidney and urinary tract defects⁸²⁻⁸⁵. Furthermore, Chapman and colleagues showed that
383 knockout of *Tbx6*^{-/-} caused defects in mesodermal and neuronal differentiation early in
384 development, leading to abnormal vascular, tail bud, and neural tube morphology⁸⁶. These
385 observations further support our findings that most fly homologs of CNV genes have a global
386 role in development that could account for the observed non-neuronal phenotypes.

387 *Second*, based on tissue-specific phenotypes, we identified fly homologs of CNV genes
388 that are key regulators of conserved cellular processes important for development. For example,
389 9/10 homologs with severe or lethal adult wing phenotypes also exhibited defects in cell
390 proliferation and apoptosis during development. In fact, we found concordance between cellular
391 processes affected by wing and eye-specific knockdown of homologs of genes within 16p11.2
392 and 3q29 regions, including decreased proliferation for *MAPK3/rl* and increased apoptosis for
393 *NCBP2/Cbp20* and *DLG1/dlg1*^{41,42}. While eye-specific knockdown of *BDHI/CG8888* showed
394 decreased cell proliferation in larval eye discs⁴², we found increased cell proliferation with wing-
395 specific knockdown, suggesting a tissue-specific effect for this gene. Notably, at least one fly
396 homolog per CNV region showed defects in cell proliferation or apoptosis, suggesting that these
397 conserved cellular processes may be relevant to CNV pathogenicity. For example, *ATXN2L/Atx2*,
398 *SH2B1/Lnk*, and *CCDC101/Sgf29* each showed decreased proliferation and increased apoptosis,
399 suggesting an underlying common conserved cellular mechanism for the distal 16p11.2 deletion.
400 Furthermore, a subset of these genes also disrupted multiple signaling pathways, indicating a
401 potential role for these genes as key regulators of developmental processes. We specifically
402 identified five genes whose knockdown caused disruptions of Wnt, Notch, and hedgehog
403 signaling pathways. Each of these genes have important roles in cell cycle regulation, apoptosis,

404 transcription, or RNA processing, based on Gene Ontology annotations^{87,88}. In fact, we found
405 that the RNA transport protein *NCBP2/Cbp20*⁸⁹, which we recently identified as a key modifier
406 gene for the 3q29 deletion⁴², interfaced with all three signaling pathways. Furthermore, *AATF*
407 disrupts apoptosis and promotes cell cycle progression through displacement of HDAC1⁹⁰⁻⁹²,
408 while *PPP4C* promotes spindle organization at the centromeres during mitosis⁹³. While we only
409 evaluated the role of these genes towards development in a single fly tissue, our additional
410 analysis of human gene interaction networks showed strong connectivity between the CNV
411 genes and signaling pathways in multiple neuronal and non-neuronal human tissues. In fact, cell
412 cycle genes were enriched among the connector genes in all three tissue-specific networks,
413 further emphasizing the role of cell cycle processes towards developmental phenotypes. Notably,
414 we also observed certain biological processes enriched among connector genes that were specific
415 to neuronal or non-neuronal tissues, indicating that haploinsufficiency of genes within CNV
416 regions may disrupt different biological processes in a tissue-specific manner.

417 *Overall*, we show that fly homologs of most CNV genes contribute towards global
418 developmental phenotypes, although exactly how they contribute toward such phenotypes varies
419 between neuronal and non-neuronal tissues. Previous functional studies for CNV disorders have
420 focused primarily on identifying candidate genes for the observed neuronal phenotypes. In this
421 study, we identified several homologs of CNV genes that are responsible for non-neuronal
422 phenotypes, as well as novel associations between these genes and conserved biological
423 processes and pathways. We therefore propose that multiple genes within each CNV disrupt
424 global and tissue-specific processes during development and contribute to the wide range of non-
425 neuronal phenotypes associated with CNV disorders (**Fig. 10**). This multigenic model for non-
426 neuronal phenotypes in CNV disorders is in line with our previous model for neuronal

427 phenotypes of these disorders, as opposed to models where individual causative genes are
428 responsible for specific phenotypes^{41,42,94}. Our study further exemplifies the utility of evaluating
429 non-neuronal phenotypes in addition to neuronal phenotypes in models of individual genes and
430 CNV regions associated with developmental disorders, including future studies in mammalian or
431 cellular model systems. Further studies exploring how CNV genes interact with each other and
432 with other developmental pathways could more fully explain the conserved mechanisms
433 underlying global developmental defects and identify potential therapeutic targets for these
434 disorders.

435 METHODS

436 Fly stocks and genetics

437 We tested 59 *Drosophila* homologs for 130 human genes that span across 10 pathogenic CNV
438 regions associated with neurodevelopmental disorders (1q21.1, 3q29, 7q11.23, 15q11.2, 15q13.3,
439 16p11.2, distal 16p11.2, 16p12.1, 16p13.11, and 17q12)²² (**Supp. Data 1**). In addition, we
440 evaluated fly homologs of 20 human genes known to be involved in neurodevelopmental
441 disorders^{60,95} (**Supp. Data 1**). These include genes involved in beta-catenin signaling pathway (5
442 genes), core genes implicated in neurodevelopmental disorders (8 genes), and genes associated
443 with microcephaly (7 genes)⁹⁶. We used the DRSC Integrative Ortholog Prediction Tool
444 (DIOPT, v.7.1) to identify the fly homologs for each human gene⁵³ (**Supp. Data 1**).

445 To knockdown individual genes in specific tissues, we used RNA interference (RNAi)
446 and the *UAS-GAL4* system (**Fig. 2A**), a well-established tool that allows for tissue-specific
447 expression of a gene of interest⁹⁷. RNAi lines were obtained from Vienna *Drosophila* Resource
448 Center (VDRC) that include both GD and KK lines. We tested a total of 136 lines in our final
449 data analysis (**Supp. Data 9**), after eliminating KK lines with additional insertion that drives the
450 overexpression of the Tiptop (*tio*) transcription factor^{98,99}. A complete list of stock numbers and
451 full genotypes for all RNAi lines used in this study is presented in **Supp. Data 9**. We used the
452 *bx^{MS1096}-GAL4/FM7c;;UAS-Dicer2/TM6B* driver for wing-specific knockdown and *w¹¹¹⁸;GMR-*
453 *GAL4;UAS-Dicer2* driver (Claire Thomas, Penn State University) for eye-specific knockdown of
454 RNAi lines. Ubiquitous knockdown experiments were performed using the *w;da-GAL4;+* driver
455 (Scott Selleck, Penn State University). For all experiments, we used appropriate GD (*w¹¹¹⁸,*
456 *VDRC# 60000*) or KK (*y,w¹¹¹⁸; P{attP,y⁺,w³}*, *VDRC# 60100*) lines as controls to compare
457 against lines with knockdown of individual homologs. All fly lines were reared on standard yeast

458 *Drosophila* medium at room temperature. All crosses were set and maintained at 25°C, except
459 for the eye knockdown experiments which were maintained at 30°C.

460

461 **Phenotypic analysis of adult wing images**

462 Adult progeny were isolated from crosses between RNAi lines and *bx^{MS1096}-GAL4* driver shortly
463 after eclosion, and kept at 25°C until day 2-5 (**Fig. 2A**). At that point, the progeny were frozen at
464 -80°C, and were then moved to -20°C prior to imaging and storage. Approximately 20-25
465 progeny, both male and female, were collected for each RNAi line tested. The adult wings were
466 plucked from frozen flies and mounted on a glass slide. The slides were covered with a coverslip
467 and sealed using clear nail polish. Adult wing images were captured using a Zeiss Discovery
468 V20 stereoscope (Zeiss, Thornwood, NY, USA), with a ProgRes Speed XT Core 3 camera and
469 CapturePro v.2.8.8 software (Jenoptik AG, Jena, Germany) at 40X magnification.

470 For each non-lethal RNAi line, we scored the adult wing images for five qualitative
471 phenotypes, including wrinkled wing, discoloration, missing veins, ectopic veins, and bristle
472 planar polarity defects, on a scale of 1 (no phenotype) to 5 (lethal) (**Fig. 3C**). Lines showing
473 severely wrinkled wings or lethality were scored as 4 (severe) or 5 (lethal) for all five
474 phenotypes. We calculated the frequency of each phenotypic score (i.e. mild bristle polarity,
475 moderate discoloration) across all of the wing images for each line (**Fig. 3A-B**), and then
476 performed k-means clustering of these values to generate five clusters for overall wing
477 phenotypes (**Fig. 2C**). For quantitative analysis of wing phenotypes, we used the Fiji ImageJ
478 software¹⁰⁰ to calculate the wing area using the Measure Area tool, and calculated the lengths of
479 longitudinal veins L2, L3, L4, and L5 as well as the anterior and posterior crossveins (ACV and
480 PCV), by tracing individual veins using the Segmented Line tool (**Fig. 4A, Supp. Data 2**). We

481 determined discordant homologs when RNAi lines for the same homologs showed inconsistent
482 wing phenotypes. For each homolog with multiple RNAi lines, we checked discordance among
483 RNAi lines for no phenotype versus any qualitative or quantitative phenotypes, followed by
484 discordance for small or large wing measurement phenotypes (**Supp. Data 3**).

485

486 **Phenotypic analysis of adult eye images**

487 We crossed RNAi lines with *GMR-GAL4* to achieve eye-specific knockdown of homologs of
488 CNV and known neurodevelopmental genes. Adult 2-3-day old female progenies from the
489 crosses were collected, immobilized by freezing at -80°C, and then moved to -20°C prior to
490 imaging and storage. Flies were mounted on Blu-tac (Bostik Inc, Wauwatosa, WI, USA) and
491 imaged using an Olympus BX53 compound microscope with LMPLan N 20X air objective using
492 a DP73 c-mount camera at 0.5X magnification (Olympus Corporation, Tokyo, Japan). CellSens
493 Dimension software (Olympus Corporation, Tokyo, Japan) was used to capture the eye images,
494 which were then stacked using the Zerene Stacker software (Zerene Systems LLC, Richland,
495 WA, USA). All eye images presented in this study are maximum projections of 20 consecutive
496 optical z-sections, at a z-step size of 12.1µm. Finally, we used our computational method called
497 *Flynotyper* (<https://flynotyper.sourceforge.net>) to quantify the degree of rough eye phenotypes
498 present due to knockdown of homologs of CNV or neurodevelopmental genes⁶⁰. *Flynotyper*
499 scores for homologs of 16p11.2 and 3q29, as well as select core neurodevelopmental genes, were
500 derived from our previous studies^{41,42,60}.

501

502

503

504 **Immunohistochemistry**

505 Wing imaginal discs from third instar larvae were dissected in 1X PBS. The tissues were fixed
506 using 4% paraformaldehyde and blocked using 1% bovine serum albumin (BSA). The wing discs
507 were incubated with primary antibodies using appropriate dilutions overnight at 4°C. We used
508 the following primary antibodies: mouse monoclonal anti-pHistone3 (S10) (1:100 dilutions, Cell
509 Signaling 9706L), rabbit polyclonal anti-cleaved *Drosophila* Dcp1 (Asp216) (1:100 dilutions,
510 Cell Signaling 9578S), mouse monoclonal anti-Wingless (1:200 dilutions, DSHB, 4D4), mouse
511 monoclonal anti-Patched (1:50 dilutions, DSHB, *Drosophila* Ptc/APA1), mouse monoclonal
512 anti-Engrailed (1:50 dilutions, DSHB, 4D9), and mouse monoclonal anti-Delta (1:50 dilutions,
513 DSHB, C594.9B). Following incubation with primary antibodies, the wing discs were washed
514 and incubated with secondary antibodies at 1:200 dilution for two hours at room temperature.
515 We used the following secondary antibodies: Alexa Fluor 647 dye goat anti-mouse (A21235,
516 Molecular Probes by Invitrogen/Life Technologies), Alexa Fluor 568 dye goat anti-rabbit
517 (A11036, Molecular Probes by Invitrogen/Life Technologies), and Alexa Fluor 568 dye goat
518 anti-mouse (A11031, Molecular Probes by Invitrogen/Life Technologies). All washes and
519 antibody dilutions were made using 0.3% PBS with Triton-X.

520 Third instar larvae wing imaginal discs were mounted in Prolong Gold antifade reagent
521 with DAPI (Thermo Fisher Scientific, P36930) for imaging using an Olympus Fluoview FV1000
522 laser scanning confocal microscope (Olympus America, Lake Success, NY). Images were
523 acquired using FV10-ASW 2.1 software (Olympus, Waltham, MA, USA). Composite z-stack
524 images were analyzed using the Fiji ImageJ software¹⁰⁰. To calculate the number of pH3 positive
525 cells within the wing pouch area of the wing discs, we used the AnalyzeParticles function in
526 ImageJ, while manual counting was used to quantify Dcp1 positive cells. We note that cell

527 proliferation and apoptosis staining for *NCBP2/Cbp20*, *DLG1/dlg1*, *BDH1/CG8888*, and
528 *FBXO45/Fsn* were previously published⁴².

529

530 **Statistical analysis**

531 Significance for the wing area and vein length measurements, cell counts for proliferation and
532 apoptosis, and *Flynotyper* scores were compared to appropriate GD or KK controls using one-
533 tailed or two-tailed Mann-Whitney tests. P-values for each set of experiments were corrected for
534 multiple testing using Benjamini-Hochberg correction. All statistical and clustering analysis was
535 performed using R v.3.6.1 (R Center for Statistical Computing, Vienna, Austria). Details for the
536 statistical tests performed for each dataset are provided in **Supp. Data 10**.

537

538 **Expression data analysis**

539 We obtained tissue-specific expression data for fly homologs of CNV genes from the FlyAtlas
540 Anatomical Microarray dataset⁶². Raw FPKM (fragments per kilobase of transcript per million
541 reads) expression values for each tissue were categorized as follows: <10, no expression; 10-100,
542 low expression; 100-500, moderate expression; 500-1000, high expression; and >1000, very high
543 expression (**Supp. Data 6**). The median expression among midgut, hindgut, Malpighian tube,
544 and (for adult only) crop tissues was used to represent the overall gut expression. We similarly
545 obtained human tissue-specific expression data for CNV genes from the GTEx Consortium v.1.2
546 RNA-Seq datasets⁶⁴. Median TPM (transcripts per million reads) expression values for each
547 tissue were categorized as follows: <3, no expression; 3-10, low expression; 10-25, moderate
548 expression; 25-100, high expression; and >100, very high expression (**Supp. Data 6**). The
549 median expression among all brain and heart sub-tissues was used to represent brain and heart

550 expression, while the median expression among all colon, esophagus, small intestine, and
551 stomach sub-tissues was used to represent digestive tract expression. Preferential gene
552 expression for a particular tissue within the GTEx dataset was determined if the expression
553 values for that tissue were greater than the third quartile of all tissue expression values for that
554 gene, plus 1.5 times the interquartile range. Venn diagrams were generated using the Venny
555 webtool (<http://bioinfogp.cnb.csic.es/tools/venny>) (Supp. Fig. 3).

556

557 **Network analysis**

558 We obtained human tissue-specific gene interaction networks for brain, heart, and kidney tissues
559 from the GIANT network database⁸⁰ within HumanBase (<https://hb.flatironinstitute.org>). These
560 networks were built by training a Bayesian classifier based on tissue-specific gene co-expression
561 datasets, which then assigned a posterior probability for interactions between each pair of genes
562 within the genome for a particular tissue. We downloaded the “Top edge” version of each tissue-
563 specific network, and extracted all gene pairs with posterior probabilities >0.2 to create sub-
564 networks containing the top ~0.5% tissue-specific interactions. Next, we identified the shortest
565 paths in each sub-network between human CNV genes whose fly homologs disrupted signaling
566 pathways in the larval wing disc and human genes within each disrupted pathway, using the
567 inverse of the posterior probability as weights for each edge in the network. Gene sets from the
568 human Notch (KEGG:map04330), Wnt (KEGG:map04310) and Hedgehog pathways
569 (KEGG:map04340) were curated from the Kyoto Encyclopedia of Genes and Genomes (KEGG)
570 pathway database¹⁰¹. Using the NetworkX Python package¹⁰², we calculated the shortest distance
571 between each CNV gene and pathway gene, and identified connecting genes that were within
572 each of the shortest paths for the three tissue-specific networks. We further tested for enrichment

573 of Gene Ontology (GO) terms (PantherDB GO-Slim) among the connector genes using the
574 PantherDB Gene List Analysis tool¹⁰³. Lists of the shortest paths and connector genes in each
575 tissue-specific network, as well as enriched GO terms for sets of connector genes, are provided
576 in **Supp. Data 8**. Gene networks were visualized using Cytoscape v.3.7.2¹⁰⁴ using an edge-
577 weighted spring embedded layout.

578

579 **Mouse and human phenotypic data analysis**

580 Phenotypic data for mouse models of CNV gene homologs, categorized using top-level
581 Mammalian Phenotype Ontology terms, were obtained from the Mouse Genome Informatics
582 (MGI) database⁸¹ (**Supp. Data 4**). Phenotypic data for human carriers of pathogenic CNVs were
583 obtained from the DECIPHER public database⁹. Clinical phenotypes for each CNV carrier were
584 categorized by top-level Human Phenotype Ontology terms¹⁰⁵ using the Orange3 Bioinformatics
585 software library (<https://orange-bioinformatics.readthedocs.io>), and the frequency of individuals
586 carrying each top-level phenotype term was calculated for each of the ten tested pathogenic
587 CNVs.

588

589 **DATA AVAILABILITY**

590 All data supporting the findings of this study are available within the paper and its
591 supplementary information files.

592

593 **CODE AVAILABILITY**

594 All source code for data analysis in this manuscript, including scripts for k-means clustering of
595 fly phenotypes, network connectivity of CNV and developmental pathway genes, and extraction
596 of top-level human phenotype terms, are available on the Girirajan lab GitHub page at
597 https://github.com/girirajanlab/CNV_wing_project.

598

599 **ACKNOWLEDGEMENTS**

600 The authors thank members of the Girirajan Lab for their helpful discussions and comments on
601 the manuscript. This study makes use of data generated by the DECIPHER community. A full
602 list of centers who contributed to the generation of the data is available from
603 <http://decipher.sanger.ac.uk> and via email from decipher@sanger.ac.uk. Funding for the project
604 was provided by the Wellcome Trust. This work was supported by NIH R01-GM121907 and
605 resources from the Huck Institutes of the Life Sciences to S.G., and NIH T32-GM102057 to M.J.

606

607 **CONTRIBUTIONS**

608 T.Y., M.J., S.Y., and S.G. designed the study. T.Y., S.Y., L.P., S.K., D.J.G., A.S., Y.M., J.I., and
609 Z.C.L. performed the functional experiments. T.Y. and M.J. performed the expression and
610 network experiments. T.Y., M.J., and S.G. analyzed the data and wrote the manuscript with input
611 from all authors.

612 **COMPETING OF INTERESTS**

613 The authors declare that they have no competing interests.

614 **REFERENCES**

- 615
- 616 1. Girirajan, S., Campbell, C. D. & Eichler, E. E. Human Copy Number Variation and
617 Complex Genetic Disease. *Annu. Rev. Genet.* **45**, 203–226 (2011).
 - 618 2. Malhotra, D. & Sebat, J. CNVs: harbingers of a rare variant revolution in psychiatric
619 genetics. *Cell* **148**, 1223–1241 (2012).
 - 620 3. Cooper, G. M. *et al.* A copy number variation morbidity map of developmental delay. *Nat.*
621 *Genet.* **43**, 838–846 (2011).
 - 622 4. Zhang, F., Gu, W., Hurles, M. E. & Lupski, J. R. Copy Number Variation in Human
623 Health, Disease, and Evolution. *Annu. Rev. Genomics Hum. Genet.* **10**, 451–481 (2009).
 - 624 5. Greenway, S. C. *et al.* De novo copy number variants identify new genes and loci in
625 isolated sporadic tetralogy of Fallot. *Nat. Genet.* **41**, 931–935 (2009).
 - 626 6. Glessner, J.T. *et al.* Increased Frequency of De Novo Copy Number Variations in
627 Congenital Heart Disease by Integrative Analysis of SNP Array and Exome Sequence
628 Data. *Circ Res.* **115**, 884–896 (2014).
 - 629 7. Sanna-Cherchi, S. *et al.* Copy-number disorders are a common cause of congenital kidney
630 malformations. *Am. J. Hum. Genet.* **91**, 987–997 (2012).
 - 631 8. Zahnleiter, D. *et al.* Rare copy number variants are a common cause of short stature. *PLoS*
632 *Genet.* **9**, e1003365 (2013).
 - 633 9. Firth, H. V. *et al.* DECIPHER: Database of Chromosomal Imbalance and Phenotype in
634 Humans Using Ensembl Resources. *Am. J. Hum. Genet.* **84**, 524–533 (2009).
 - 635 10. Mefford, H. C. *et al.* Recurrent rearrangements of chromosome 1q21.1 and variable
636 pediatric phenotypes. *N. Engl. J. Med.* **359**, 1685–99 (2008).
 - 637 11. Brunetti-Pierrri, N. *et al.* Recurrent reciprocal 1q21.1 deletions and duplications associated
638 with microcephaly or macrocephaly and developmental and behavioral abnormalities. *Nat.*
639 *Genet.* **40**, 1466–1471 (2008).
 - 640 12. Christiansen, J. *et al.* Chromosome 1q21.1 contiguous gene deletion is associated with
641 congenital heart disease. *Circ. Res.* **94**, 1429–35 (2004).
 - 642 13. Pober, B. R. Williams-Beuren syndrome. *N. Engl. J. Med.* **362**, 239–52 (2010).
 - 643 14. Ewart, A. K. *et al.* A human vascular disorder, supravalvular aortic stenosis, maps to
644 chromosome 7. *Proc. Natl. Acad. Sci. U. S. A.* **90**, 3226–30 (1993).
 - 645 15. Romeo, S. *et al.* Search for genetic variants of the SYNTAXIN 1A (STX1A) gene: The -
646 352 A>T variant in the STX1A promoter associates with impaired glucose metabolism in
647 an Italian obese population. *Int. J. Obes.* **32**, 413–420 (2008).
 - 648 16. Frangiskakis, J. M. *et al.* LIM-kinase1 hemizyosity implicated in impaired visuospatial
649 constructive cognition. *Cell* **86**, 59–69 (1996).
 - 650 17. Tassabehji, M. *et al.* GTF2IRD1 in craniofacial development of humans mice. *Science*
651 **310**, 1184–1187 (2005).
 - 652 18. Lindsay, E. A. *et al.* Tbx1 haploinsufficiency in the DiGeorge syndrome region causes
653 aortic arch defects in mice. *Nature* **410**, 97–101 (2001).
 - 654 19. Mefford, H. C. *et al.* Recurrent reciprocal genomic rearrangements of 17q12 are
655 associated with renal disease, diabetes, and epilepsy. *Am. J. Hum. Genet.* **81**, 1057–1069
656 (2007).
 - 657 20. Clissold, R. L. *et al.* Chromosome 17q12 microdeletions but not intragenic HNF1B
658 mutations link developmental kidney disease and psychiatric disorder. *Kidney Int.* **90**,
659 203–11 (2016).

- 660 21. Weiss, L. A. *et al.* Association between Microdeletion and Microduplication at 16p11.2
661 and Autism. *N. Engl. J. Med.* **358**, 667–675 (2008).
- 662 22. Girirajan, S. *et al.* Phenotypic Heterogeneity of Genomic Disorders and Rare Copy-
663 Number Variants. *N. Engl. J. Med.* **367**, 1321–1331 (2012).
- 664 23. Bernier, R. *et al.* Disruptive CHD8 Mutations Define a Subtype of Autism Early in
665 Development. *Cell* **158**, 263–276 (2014).
- 666 24. Ostergaard, P. *et al.* Mutations in KIF11 cause autosomal-dominant microcephaly variably
667 associated with congenital lymphedema and chorioretinopathy. *Am. J. Hum. Genet.* **90**,
668 356–62 (2012).
- 669 25. Horev, G. *et al.* Dosage-dependent phenotypes in models of 16p11.2 lesions found in
670 autism. *Proc. Natl. Acad. Sci.* **108**, 17076–17081 (2011).
- 671 26. Pucilowska, J. *et al.* The 16p11.2 Deletion Mouse Model of Autism Exhibits Altered
672 Cortical Progenitor Proliferation and Brain Cytoarchitecture Linked to the ERK MAPK
673 Pathway. *J. Neurosci.* **35**, 3190–3200 (2015).
- 674 27. Portmann, T. *et al.* Behavioral abnormalities and circuit defects in the basal ganglia of a
675 mouse model of 16p11.2 deletion syndrome. *Cell Rep.* **7**, 1077–1092 (2014).
- 676 28. Rutkowski, T. P. *et al.* Behavioral changes and growth deficits in a CRISPR engineered
677 mouse model of the schizophrenia-associated 3q29 deletion. *Mol. Psychiatry* (2019)
678 doi:10.1038/s41380-019-0413-5.
- 679 29. Baba, M. *et al.* Psychiatric-disorder-related behavioral phenotypes and cortical
680 hyperactivity in a mouse model of 3q29 deletion syndrome. *Neuropsychopharmacology*
681 **44**, 2125–2135 (2019).
- 682 30. Arbogast, T. *et al.* Reciprocal Effects on Neurocognitive and Metabolic Phenotypes in
683 Mouse Models of 16p11.2 Deletion and Duplication Syndromes. *PLoS Genet.* **12**,
684 e1005709 (2016).
- 685 31. Haller, M., Au, J., O’Neill, M. & Lamb, D. J. 16p11.2 transcription factor MAZ is a
686 dosage-sensitive regulator of genitourinary development. *Proc. Natl. Acad. Sci.* **115**,
687 E1849–E1858 (2018).
- 688 32. Yadav, S. *et al.* TAOK2 Kinase Mediates PSD95 Stability and Dendritic Spine Maturation
689 through Septin7 Phosphorylation. *Neuron* **93**, 379–393 (2017).
- 690 33. Richter, M. *et al.* Altered TAOK2 activity causes autism-related neurodevelopmental and
691 cognitive abnormalities through RhoA signaling. *Mol. Psychiatry* **24**, 1329–1350 (2019).
- 692 34. Golzio, C. *et al.* KCTD13 is a major driver of mirrored neuroanatomical phenotypes of the
693 16p11.2 copy number variant. *Nature* **485**, 363–367 (2012).
- 694 35. Escamilla, C. O. *et al.* Kctd13 deletion reduces synaptic transmission via increased RhoA.
695 *Nature* **551**, 227–231 (2017).
- 696 36. Ip, J. P. K. *et al.* Major vault protein, a candidate gene in 16p11.2 microdeletion
697 syndrome, is required for the homeostatic regulation of visual cortical plasticity. *J.*
698 *Neurosci.* **38**, 2017–2034 (2018).
- 699 37. Dickinson, M. E. *et al.* High-throughput discovery of novel developmental phenotypes.
700 *Nature* **537**, 508–514 (2016).
- 701 38. Wangler, M. F., Yamamoto, S. & Bellen, H. J. Fruit flies in biomedical research. *Genetics*
702 **199**, 639–653 (2015).
- 703 39. Chien, S. Homophila: human disease gene cognates in *Drosophila*. *Nucleic Acids Res.* **30**,
704 149–151 (2002).
- 705 40. Reiter, L. T., Potocki, L., Chien, S., Gribskov, M. & Bier, E. A systematic analysis of

- 706 human disease-associated gene sequences in *Drosophila melanogaster*. *Genome Res.* **11**,
707 1114–1125 (2001).
- 708 41. Iyer, J. *et al.* Pervasive genetic interactions modulate neurodevelopmental defects of the
709 autism-associated 16p11.2 deletion in *Drosophila melanogaster*. *Nat. Commun.* **9**, 2548
710 (2018).
- 711 42. Singh, M. D. *et al.* NCBP2 modulates neurodevelopmental defects of the 3q29 deletion in
712 *Drosophila* and *X. laevis* models. *bioRxiv* 614750 (2019) doi:10.1101/614750.
- 713 43. Molnar, C. *et al.* Signalling Pathways in Development and Human Disease: A *Drosophila*
714 Wing Perspective. in *Human Genetic Diseases* (InTech, 2011). doi:10.5772/23858.
- 715 44. Dworkin, I. & Gibson, G. Epidermal growth factor receptor and transforming growth
716 factor- β signaling contributes to variation for wing shape in *Drosophila melanogaster*.
717 *Genetics* **173**, 1417–1431 (2006).
- 718 45. Testa, N. D. & Dworkin, I. The sex-limited effects of mutations in the EGFR and TGF- β
719 signaling pathways on shape and size sexual dimorphism and allometry in the *Drosophila*
720 wing. *Dev. Genes Evol.* **226**, 159–171 (2016).
- 721 46. Yan, S. J., Gu, Y., Li, W. X. & Fleming, R. J. Multiple signaling pathways and a selector
722 protein sequentially regulate *Drosophila* wing development. *Development* **131**, 285–298
723 (2004).
- 724 47. Strigini, M. & Cohen, S. M. A Hedgehog activity gradient contributes to AP axial
725 patterning of the *Drosophila* wing. *Development* **124**, 4697–4705 (1997).
- 726 48. Diaz de la Loza, M. C. & Thompson, B. J. Forces shaping the *Drosophila* wing. *Mech.*
727 *Dev.* **144**, 23–32 (2017).
- 728 49. Bier, E. *Drosophila*, the golden bug, emerges as a tool for human genetics. *Nat. Rev.*
729 *Genet.* **6**, 9–23 (2005).
- 730 50. Wu, Y. *et al.* A *Drosophila* model for Angelman syndrome. *Proc. Natl. Acad. Sci.* **105**,
731 12399–12404 (2008).
- 732 51. Yamamoto, S. *et al.* A *Drosophila* genetic resource of mutants to study mechanisms
733 underlying human genetic diseases. *Cell* **159**, 200–214 (2014).
- 734 52. Kochinke, K. *et al.* Systematic Phenomics Analysis Deconvolutes Genes Mutated in
735 Intellectual Disability into Biologically Coherent Modules. *Am. J. Hum. Genet.* **98**, 149–
736 164 (2016).
- 737 53. Hu, Y. *et al.* An integrative approach to ortholog prediction for disease-focused and other
738 functional studies. *BMC Bioinformatics* **12**, 357 (2011).
- 739 54. Capdevila, J. & Guerrero, I. Targeted expression of the signaling molecule
740 decapentaplegic induces pattern duplications and growth alterations in *Drosophila* wings.
741 *EMBO J.* **13**, 4459–4468 (1994).
- 742 55. Lindström, R., Lindholm, P., Palgi, M., Saarma, M. & Heino, T. I. In vivo screening
743 reveals interactions between *Drosophila* Manf and genes involved in the mitochondria and
744 the ubiquinone synthesis pathway. *BMC Genet.* **18**, 52 (2017).
- 745 56. Nielsen, J. *et al.* A mouse model of the schizophrenia-associated 1q21.1 microdeletion
746 syndrome exhibits altered mesolimbic dopamine transmission. *Transl. Psychiatry* **7**, 1261
747 (2017).
- 748 57. Huang, H. *et al.* PTEN affects cell size, cell proliferation and apoptosis during *Drosophila*
749 eye development. *Development* **126**, 5365–5372 (1999).
- 750 58. Toyo-oka, K. *et al.* Protein phosphatase 4 catalytic subunit regulates Cdk1 activity and
751 microtubule organization via NDEL1 dephosphorylation. *J. Cell Biol.* **180**, 1133–1147

- 752 (2008).
- 753 59. Ohsugi, M. *et al.* Kid-Mediated Chromosome Compaction Ensures Proper Nuclear
754 Envelope Formation. *Cell* **132**, 771–782 (2008).
- 755 60. Iyer, J. *et al.* Quantitative assessment of eye phenotypes for functional genetic studies
756 using *Drosophila melanogaster*. *G3 Genes, Genomes, Genet.* **6**, 1427–1437 (2016).
- 757 61. Rosenberg, M. J. *et al.* Mutant deoxynucleotide carrier is associated with congenital
758 microcephaly. *Nat. Genet.* **32**, 175–179 (2002).
- 759 62. Chintapalli, V. R., Wang, J. & Dow, J. A. T. Using FlyAtlas to identify better *Drosophila*
760 *melanogaster* models of human disease. *Nat. Genet.* **39**, 715–720 (2007).
- 761 63. Claes, L. *et al.* De novo mutations in the sodium-channel gene SCN1A cause severe
762 myoclonic epilepsy of infancy. *Am. J. Hum. Genet.* **68**, 1327–1332 (2001).
- 763 64. Ardlie, K. G. *et al.* The Genotype-Tissue Expression (GTEx) pilot analysis: Multitissue
764 gene regulation in humans. *Science* **348**, 648–660 (2015).
- 765 65. Ernst, C. Proliferation and Differentiation Deficits are a Major Convergence Point for
766 Neurodevelopmental Disorders. *Trends Neurosci.* **39**, 290–299 (2016).
- 767 66. Marchetto, M. C. *et al.* Altered proliferation and networks in neural cells derived from
768 idiopathic autistic individuals. *Mol. Psychiatry* **22**, 820–835 (2017).
- 769 67. Wei, H., Alberts, I. & Li, X. The apoptotic perspective of autism. *Int. J. Dev. Neurosci.*
770 **36**, 13–18 (2014).
- 771 68. Hartl, T. A. & Scott, M. P. Wing tips: The wing disc as a platform for studying Hedgehog
772 signaling. *Methods* **68**, 199–206 (2014).
- 773 69. de Celis, J. F. & García-Bellido, A. Roles of the Notch gene in *Drosophila* wing
774 morphogenesis. *Mech. Dev.* **46**, 109–122 (1994).
- 775 70. Raftery, L. A. & Umulis, D. M. Regulation of BMP activity and range in *Drosophila* wing
776 development. *Curr. Opin. Cell Biol.* **24**, 158–65 (2012).
- 777 71. Diaz-Benjumea, F. J. & Cohen, S. M. Serrate signals through Notch to establish a
778 Wingless-dependent organizer at the dorsal/ventral compartment boundary of the
779 *Drosophila* wing. *Development* **121**, 4215–4225 (1995).
- 780 72. Becam, I. & Milán, M. A permissive role of Notch in maintaining the DV affinity
781 boundary of the *Drosophila* wing. *Dev. Biol.* **322**, 190–8 (2008).
- 782 73. Zecca, M., Basler, K. & Struhl, G. Sequential organizing activities of engrailed, hedgehog
783 and decapentaplegic in the *Drosophila* wing. *Development* **121**, 2265–2278 (1995).
- 784 74. Tabata, T. & Kornberg, T. B. Hedgehog is a signaling protein with a key role in patterning
785 *Drosophila* imaginal discs. *Cell* **76**, 89–102 (1994).
- 786 75. O’Roak, B. J. *et al.* Sporadic autism exomes reveal a highly interconnected protein
787 network of de novo mutations. *Nature* **485**, 246–250 (2012).
- 788 76. Hahn, H. *et al.* Mutations of the human homolog of *Drosophila* patched in the nevoid
789 basal cell carcinoma syndrome. *Cell* **85**, 841–851 (1996).
- 790 77. Johnson, R. L. *et al.* Human homolog of patched, a candidate gene for the basal cell nevus
791 syndrome. *Science* **272**, 1668–1671 (1996).
- 792 78. Swarup, S., Pradhan-Sundd, T. & Verheyen, E. M. Genome-wide identification of
793 phospho-regulators of Wnt signaling in *Drosophila*. *Development* **142**, 1502–1515 (2015).
- 794 79. Six, E. M. *et al.* The Notch ligand Delta1 recruits Dlg1 at cell-cell contacts and regulates
795 cell migration. *J. Biol. Chem.* **279**, 55818–55826 (2004).
- 796 80. Greene, C. S. *et al.* Understanding multicellular function and disease with human tissue-
797 specific networks. *Nat. Genet.* **47**, 569–576 (2015).

- 798 81. Bult, C. J. *et al.* Mouse Genome Database (MGD) 2019. *Nucleic Acids Res.* **47**, D801–
799 D806 (2019).
- 800 82. Zhou, W. *et al.* GluR1 controls dendrite growth through its binding partner, SAP97. *J.*
801 *Neurosci.* **28**, 10220–10233 (2008).
- 802 83. Iizuka-Kogo, A., Ishidao, T., Akiyama, T. & Senda, T. Abnormal development of
803 urogenital organs in Dlg1-deficient mice. *Development* **134**, 1799–1807 (2007).
- 804 84. Mahoney, Z. X. *et al.* Discs-large homolog 1 regulates smooth muscle orientation in the
805 mouse ureter. *Proc. Natl. Acad. Sci.* **103**, 19872–19877 (2006).
- 806 85. Caruana, G. & Bernstein, A. Craniofacial dysmorphogenesis including cleft palate in mice
807 with an insertional mutation in the discs large gene. *Mol. Cell. Biol.* **21**, 1475–83 (2001).
- 808 86. Chapman, D. L. & Papaioannou, V. E. Three neural tubes in mouse embryos with
809 mutations in the T-box gene Tbx6. *Nature* **391**, 695–697 (1998).
- 810 87. Ashburner, M. *et al.* Gene ontology: Tool for the unification of biology. *Nat. Genet.* **25**,
811 25–29 (2000).
- 812 88. The Gene Ontology Consortium. The Gene Ontology Resource: 20 years and still GOing
813 strong. *Nucleic Acids Res.* **47**, D330–D338 (2019).
- 814 89. Pabis, M., Neufeld, N., Shav-Tal, Y. & Neugebauer, K. M. Binding properties and
815 dynamic localization of an alternative isoform of the cap-binding complex subunit CBP20.
816 *Nucleus* **1**, 412–421 (2010).
- 817 90. Di Padova, M. *et al.* Che-1 arrests human colon carcinoma cell proliferation by displacing
818 HDAC1 from the p21WAF1/CIP1 promoter. *J. Biol. Chem.* **278**, 36496–504 (2003).
- 819 91. Bruno, T. *et al.* Che-1 affects cell growth by interfering with the recruitment of HDAC1
820 by Rb. *Cancer Cell* **2**, 387–399 (2002).
- 821 92. Page, G., Lödige, I., Kögel, D. & Scheidtmann, K. H. AATF, a novel transcription factor
822 that interacts with Dlk/ZIP kinase and interferes with apoptosis. *FEBS Lett.* **462**, 187–91
823 (1999).
- 824 93. Sumiyoshi, E., Sugimoto, A. & Yamamoto, M. Protein phosphatase 4 is required for
825 centrosome maturation in mitosis and sperm meiosis in *C. elegans*. *J. Cell Sci.* **115**, 1403–
826 1410 (2002).
- 827 94. Jensen, M. & Girirajan, S. An interaction-based model for neuropsychiatric features of
828 copy-number variants. *PLoS Genet.* **15**, e1007879 (2019).
- 829 95. Coe, B. P., Girirajan, S. & Eichler, E. E. A genetic model for neurodevelopmental disease.
830 *Curr. Opin. Neurobiol.* **22**, 829–836 (2012).
- 831 96. Nicholas, A. K. *et al.* The molecular landscape of ASPM mutations in primary
832 microcephaly. *J. Med. Genet.* **46**, 249–253 (2009).
- 833 97. Brand, A. H. & Perrimon, N. Targeted gene expression as a means of altering cell fates
834 and generating dominant phenotypes. *Development* **118**, 401–15 (1993).
- 835 98. Green, E. W., Fedele, G., Giorgini, F. & Kyriacou, C. P. A Drosophila RNAi collection is
836 subject to dominant phenotypic effects. *Nat. Methods* **11**, 222–223 (2014).
- 837 99. Vissers, J. H. A., Manning, S. A., Kulkarni, A. & Harvey, K. F. A Drosophila RNAi
838 library modulates Hippo pathway-dependent tissue growth. *Nat. Commun.* **7**, 10368
839 (2016).
- 840 100. Schindelin, J. *et al.* Fiji: An open-source platform for biological-image analysis. *Nat.*
841 *Methods* **9**, 676–682 (2012).
- 842 101. Kanehisa, M., Sato, Y., Furumichi, M., Morishima, K. & Tanabe, M. New approach for
843 understanding genome variations in KEGG. *Nucleic Acids Res.* **47**, D590–D595 (2019).

- 844 102. Hagberg, A. A., Schult, D. A. & Swart, P. J. Exploring network structure, dynamics, and
845 function using NetworkX. in *7th Python in Science Conference (SciPy 2008)* 11–15
846 (2008).
- 847 103. Mi, H. *et al.* PANTHER version 11: Expanded annotation data from Gene Ontology and
848 Reactome pathways, and data analysis tool enhancements. *Nucleic Acids Res.* **45**, D183–
849 D189 (2017).
- 850 104. Shannon, P. *et al.* Cytoscape: A software Environment for integrated models of
851 biomolecular interaction networks. *Genome Res.* **13**, 2498–2504 (2003).
- 852 105. Köhler, S. *et al.* Expansion of the Human Phenotype Ontology (HPO) knowledge base and
853 resources. *Nucleic Acids Res.* **47**, D1018–D1027 (2019).
854

855 **FIGURE LEGENDS**

856 **Figure 1. Phenotypic expression of CNV carriers across tissues.** Heatmap with frequencies of
857 non-neuronal developmental phenotypes observed in 1,225 human carriers of 10 pathogenic
858 CNV deletions, curated from the DECIPHER database, is shown. CNV carriers show a variety of
859 phenotypes that manifest across different tissues, including eye, limbs, muscle, and skeleton.

860

861 **Figure 2. Targeted analysis to identify global developmental phenotypes with knockdown**
862 **of homologs of CNV genes. (A)** Strategy for identifying non-neuronal phenotypes and
863 underlying cellular mechanisms for homologs of CNV and known neurodevelopmental genes
864 using the fly wing as a model system. We evaluated 59 *Drosophila* homologs of genes within 10
865 CNV regions and 20 known neurodevelopmental genes (79 total homologs). Using the *UAS-*
866 *GAL4* system with wing-specific *bx^{MS1096}* driver, we knocked down 136 individual RNAi lines
867 for the CNV and neurodevelopmental homologs, and evaluated qualitative and quantitative
868 phenotypes. We next clustered RNAi lines based on severity of qualitative phenotypes, and
869 compared adult wing phenotypes to phenotypes observed with ubiquitous and eye-specific
870 knockdown of homologs. Furthermore, we evaluated underlying cellular mechanisms for the
871 observed wing-specific phenotypes, and examined the connectivity patterns of candidate
872 homologs for developmental phenotypes in multiple human tissue-specific networks. **(B)**
873 Representative brightfield images of adult wing phenotype severity observed with knockdown of
874 homologs of CNV genes, based on clustering analysis, are shown. **(C)** Heatmap with k-means
875 clustering of qualitative phenotypes in adult female wings across 136 RNAi lines is shown. The
876 color of each cell represents the frequency of individual fly wings (n=20-25 adult wings) for
877 each RNAi line (x-axis) that show a specific severity (no phenotype, mild, moderate, severe,

878 lethal) for the five qualitative phenotypes assessed (y-axis; wrinkled wings, ectopic veins,
879 missing veins, discoloration, bristle planar polarity), as detailed in **Supp. Data 2**. Based on these
880 data, we identified clusters for no phenotype (n=75 lines), mild (n=24 lines), moderate (n=10
881 lines), severe (n=21 lines), and lethal (n=6 lines). **(D)** Summary table of qualitative and
882 quantitative adult wing phenotypes for all tested RNAi lines of homologs of CNV and
883 neurodevelopmental genes. Quantitative phenotype totals do not include lethal RNAi lines for
884 both area and vein length. In addition, L3 vein length totals do not include severe RNAi lines.
885

886 **Figure 3. Qualitative adult wing phenotypes of *Drosophila* homologs of CNV and**
887 **neurodevelopmental genes.** Heatmaps representing the five qualitative adult wing phenotypes
888 for all 136 RNAi lines, with **(A)** all 59 tested homologs for 10 CNV regions and **(B)** 20
889 homologs for neurodevelopmental genes (β -catenin, core neurodevelopmental genes, and
890 microcephaly genes), are shown. The color of each cell represents the frequency of each of the
891 five qualitative phenotypes by severity (wrinkled wings, WR; ectopic veins, EV; missing veins,
892 MV; discoloration, DC; bristle planar polarity, BP), ranging from no phenotype to lethal. **(C)**
893 Representative brightfield images of adult fly wings (scale bar = 500 μ m) with wing-specific
894 knockdown of homologs of CNV and neurodevelopmental genes showing the five assessed
895 qualitative phenotypes, including discoloration, wrinkled wings, bristle polarity, ectopic veins,
896 and missing veins are shown. The panels in the bx^{MS1096} -*GAL4* control and $C6836^{KK112485}$ images
897 highlight bristle planar polarity phenotypes for the representative images. Black arrowheads
898 highlight ectopic veins and white arrowheads highlight missing veins. Genotypes for the images
899 are: w^{1118}/bx^{MS1096} -*GAL4*;+; *UAS-Dicer2*/+, w^{1118}/bx^{MS1096} -*GAL4*; *UAS-Rph*^{GD7330} RNAi/+; *UAS-*
900 *Dicer2*/+, w^{1118}/bx^{MS1096} -*GAL4*; *UAS-CG15528*^{KK107736} RNAi/+; *UAS-Dicer2*/+, w^{1118}/bx^{MS1096} -

901 *GAL4;UAS-CG6836^{KK112485} RNAi/+; UAS-Dicer2/+*, *w¹¹¹⁸/bx^{MS1096}-GAL4;+;UAS-*
902 *CG14182^{GD2738} RNAi/UAS-Dicer2*, and *w¹¹¹⁸/bx^{MS1096}-GAL4;UAS-kis^{KK100890} RNAi/+; UAS-*
903 *Dicer2/+*.

904

905 **Figure 4. Quantitative adult wing phenotypes of *Drosophila* homologs of CNV and**

906 **neurodevelopmental genes. (A)** Representative brightfield images of adult fly wings (scale bar

907 = 500µm) with wing-specific knockdown of homologs of CNV and neurodevelopmental genes

908 with size defects are shown. The *bx^{MS1096}-GAL4* control image highlights the six veins, including

909 longitudinal veins L2, L3, L4, and L5 as well as the anterior and posterior crossveins (ACV and

910 PCV), that were measured for quantitative analysis. The dotted line in the control image

911 represents the total wing area calculated for each RNAi line. Genotypes for the images are:

912 *w¹¹¹⁸/bx^{MS1096}-GAL4;+; UAS-Dicer2/+*, *w¹¹¹⁸/bx^{MS1096}-GAL4;UAS-Fmo-2^{KK109203} RNAi/+; UAS-*

913 *Dicer2/+*, and *w¹¹¹⁸/bx^{MS1096}-GAL4;+;UAS-Trpm^{GD4541} RNAi/UAS-Dicer2*. **(B)** Boxplot of L3

914 vein lengths for knockdown of select homologs in adult fly wings (n = 9-91, *p < 0.05, two-

915 tailed Mann–Whitney test with Benjamini-Hochberg correction). Vein measurements for all

916 other longitudinal veins and crossveins (ACV and PCV) for these lines are represented in **Supp**

917 **Fig. 2. (C)** Boxplot of wing areas for knockdown of select homologs in adult fly wings (n = 9-

918 91, *p < 0.05, two-tailed Mann–Whitney test with Benjamini-Hochberg correction). All boxplots

919 indicate median (center line), 25th and 75th percentiles (bounds of box), and minimum and

920 maximum (whiskers), with red dotted lines representing the control median.

921

922 **Figure 5. Comparison of wing-specific, eye-specific, and ubiquitous knockdown of**

923 **homologs of CNV and known neurodevelopmental genes. (A)** Heatmap with the penetrance

924 of phenotypes with ubiquitous knockdown (*da-GAL4*) of select homologs of CNV genes,
925 compared to their adult wing-specific (*bx^{MS1096}-GAL4*) phenotypic severity is shown. **(B)**
926 Boxplots of *Flynotyper*-derived phenotypic scores for adult eyes with eye-specific knockdown
927 (*GMR-GAL4*) of select homologs of CNV and neurodevelopmental genes, normalized as fold-
928 change (FC) to control values (n = 7–40, *p < 0.05, one-tailed Mann–Whitney test with
929 Benjamini-Hochberg correction). The boxplots are arranged by severity of adult wing
930 phenotypes observed for each RNAi line, while the *Flynotyper* phenotypic scores are categorized
931 into four severity categories: no change (0–1.1 FC), mild (1.1–1.5 FC), moderate (1.5–2.0 FC),
932 and severe (>2.0 FC). **(C)** Boxplot showing the average eye phenotypic scores for 66 RNAi lines
933 of select homologs of CNV and neurodevelopmental genes, normalized as fold-change (FC) to
934 control values, by wing phenotypic category (n=4–30 RNAi lines per group). We did not observe
935 any significant changes in eye phenotype severity across the five wing phenotypic categories
936 (Kruskal-Wallis rank sum test, p=0.567, df = 5, $\chi^2 = 3.881$). Examples of average eye phenotypic
937 scores for RNAi lines with no phenotype (*para^{GD3392-1}*), mild (*rl^{KK115768}*), and lethal (*dlg1^{GD4689}*)
938 wing phenotype severity are highlighted in the graph. All boxplots indicate median (center line),
939 25th and 75th percentiles (bounds of box), and minimum and maximum (whiskers), with red
940 dotted lines representing the control median. **(D)** Representative brightfield adult eye (scale
941 bar = 100 μ m) and adult wing (scale bar = 500 μ m) images with tissue-specific knockdown of
942 homologs of CNV genes are shown. Genotypes for the eye images are: *w¹¹¹⁸;GMR-GAL4/+;*
943 *UAS-Dicer2/+*, *w¹¹¹⁸;GMR-GAL4/UAS-Lnk^{KK105731} RNAi*; *UAS-Dicer2/+*, *w¹¹¹⁸;GMR-*
944 *GAL4/UAS-mEFTu1^{GD16961} RNAi*; *UAS-Dicer2/+*. Genotypes for the wing images are:
945 *w¹¹¹⁸/bx^{MS1096}-GAL4;+;* *UAS-Dicer2/+*, *w¹¹¹⁸/bx^{MS1096}-GAL4;* *UAS-Lnk^{KK105731} RNAi/+;* *UAS-*
946 *Dicer2/+*, and *w¹¹¹⁸/bx^{MS1096}-GAL4;* *UAS-mEFTu1^{GD16961} RNAi/+;* *UAS-Dicer2/+*.

947 **Figure 6. Expression patterns of *Drosophila* homologs and human CNV and**
948 **neurodevelopmental genes across multiple tissues. (A)** Heatmap with expression of fly
949 homologs of select CNV and neurodevelopmental genes in multiple *Drosophila* larval and adult
950 tissues, derived from the FlyAtlas Anatomical Microarray dataset, compared with adult wing
951 phenotype severity, is shown. Expression values are grouped into no expression (<10 fragments
952 per kilobase of transcript per million reads, or FPKM), low (10–100 FPKM), moderate (100–500
953 FPKM), high (500–1000 FPKM), and very high (>1000 FPKM) expression categories. **(B)**
954 Heatmap with expression of select human CNV and neurodevelopmental genes in multiple adult
955 tissues, derived from the Genotype-Tissue Expression (GTEx) dataset v.1.2, is shown.
956 Expression values are grouped into no expression (<3 transcripts per million reads, or TPM), low
957 (3–10 TPM), moderate (10–25 TPM), high (25–100 TPM), and very high (>100 TPM)
958 expression categories. X symbols denote preferential expression in a particular tissue (see
959 Methods). Expression data for all CNV and neurodevelopmental genes are provided in **Supp.**
960 **Data 6.**

961
962 **Figure 7. *Drosophila* homologs of CNV and neurodevelopmental genes show altered levels**
963 **of apoptosis and proliferation. (A)** Larval imaginal wing discs (scale bar = 50 μ m) stained with
964 nuclear marker DAPI, apoptosis marker dcp1, and cell proliferation marker pH3 illustrate altered
965 levels of apoptosis and cell proliferation due to wing-specific knockdown of select fly homologs
966 of CNV genes. We quantified the number of stained cells within the wing pouch of the wing disc
967 (white box), which becomes the adult wing. Additional representative images of select homologs
968 are presented in **Supp Fig. 5**. Genotypes for the wing images are: $w^{1118}/bx^{MS1096}-GAL4;+; UAS-$
969 $Dicer2/+$, $w^{1118}/bx^{MS1096}-GAL4;+; UAS-Aatf^{GD7229} RNAi/UAS-Dicer2$, $w^{1118}/bx^{MS1096}-GAL4;UAS-$

970 *Pp4-19C^{GD9561}/+*; *UAS-Dicer2/+*, *w¹¹¹⁸/bx^{MS1096}-GAL4/+*; *UAS-Atx2^{GD11562} RNAi/UAS-Dicer2*,
971 and *w¹¹¹⁸/bx^{MS1096}-GAL4/+*; *UAS-Sin^{GD7027} RNAi/UAS-Dicer2*. **(B)** Box plot of dcp1-positive
972 cells in larval wing discs with knockdown of select fly homologs of CNV and
973 neurodevelopmental genes, normalized to controls (n = 7–18, *p < 0.05, two-tailed Mann–
974 Whitney test with Benjamini-Hochberg correction). We note that several RNAi lines showed
975 severe dcp1 staining across the entire wing disc and could not be quantified. The number of dcp1
976 positive cells were calculated manually. **(C)** Box plot of pH3-positive cells in the larval wing
977 discs with knockdown of select fly homologs of CNV and neurodevelopmental genes,
978 normalized to controls (n = 6–18, *p < 0.05, two-tailed Mann–Whitney test with Benjamini-
979 Hochberg correction). The number of pH3 positive cells were calculated using the
980 AnalyzeParticles function in ImageJ. All boxplots indicate median (center line), 25th and 75th
981 percentiles (bounds of box), and minimum and maximum (whiskers), with red dotted lines
982 representing the control median.

983
984 **Figure 8. Candidate *Drosophila* homologs of genes within CNV regions interact with**
985 **conserved signaling pathways.** Larval imaginal wing discs (scale bar = 50 μm) stained with **(A)**
986 wingless, **(B)** patched, **(C)** engrailed, and **(D)** delta illustrate disrupted expression patterns for
987 proteins located within the Wnt (wingless), Hedgehog (patched and engrailed), and Notch (delta)
988 signaling pathways due to wing-specific knockdown of select fly homologs of CNV and
989 neurodevelopmental genes. Dotted yellow boxes represent expected expression patterns for
990 signaling proteins in *bx^{MS1096}-GAL4* control images. White arrowheads and dotted white boxes
991 highlight disruptions in expression patterns of signaling proteins with knockdown of CNV or
992 neurodevelopmental genes. Additional representative images of select homologs are presented in

993 **Supp Fig. 7.** Genotypes for the wing images are: $w^{1118}/bx^{MS1096}-GAL4;+; UAS-Dicer2/+$,
994 $w^{1118}/bx^{MS1096}-GAL4;UAS-Pp4-19C^{GD9561}/+; UAS-Dicer2/+$, $w^{1118}/bx^{MS1096}-GAL4;UAS-$
995 $Cbp20^{KK109448}/+; UAS-Dicer2/+$, $w^{1118}/bx^{MS1096}-GAL4;+; UAS-Sin^{GD7027} RNAi/UAS-Dicer2$,
996 $w^{1118}/bx^{MS1096}-GAL4;+; UAS-Aatf^{GD7229} RNAi/UAS-Dicer2$, and $w^{1118}/bx^{MS1096}-GAL4;UAS-$
997 $Klp61F^{GD14149}/+; UAS-Dicer2/+$.

998

999 **Figure 9. Connectivity of human CNV genes with conserved signaling pathway genes in**
1000 **human tissue-specific networks. (A)** Representative diagrams of eight human CNV and
1001 neurodevelopmental genes whose fly homologs disrupt the Notch signaling pathway and 57
1002 human Notch signaling genes within kidney, heart, and brain-specific gene interaction networks
1003 are shown. Yellow nodes represent CNV and neurodevelopmental genes, pink nodes represent
1004 Notch signaling pathway genes, and green nodes represent connector genes within the shortest
1005 paths between CNV and Notch pathway genes. **(B)** Violin plots showing the average
1006 connectivity (i.e. inverse of shortest path lengths) of CNV genes to genes in Hedgehog, Notch,
1007 and Wnt signaling pathways across the tested tissue-specific networks (n=322–810 pairwise
1008 interactions, *p < 0.05, two-tailed Welch's t-test with Benjamini-Hochberg correction). **(C)**
1009 Table showing enriched clusters of Gene Ontology (GO) Biological Process terms for connector
1010 genes observed for each signaling pathway in the three tested tissue-specific networks,
1011 categorized by enrichments in ubiquitous, neuronal, and non-neuronal tissues (p<0.05, Fisher's
1012 Exact test with Benjamini-Hochberg correction).

1013

1014 **Figure 10. A multigenic model for neuronal and non-neuronal phenotypes associated with**
1015 **pathogenic CNVs.** Schematic of a multigenic model for neuronal and non-neuronal phenotypes

1016 associated with pathogenic CNVs. While a subset of genes within CNV regions contribute
1017 towards tissue-specific phenotypes, a majority of genes contribute towards both neuronal and
1018 non-neuronal phenotypes through disruption of developmental signaling pathways and global
1019 biological processes.

Figure 1

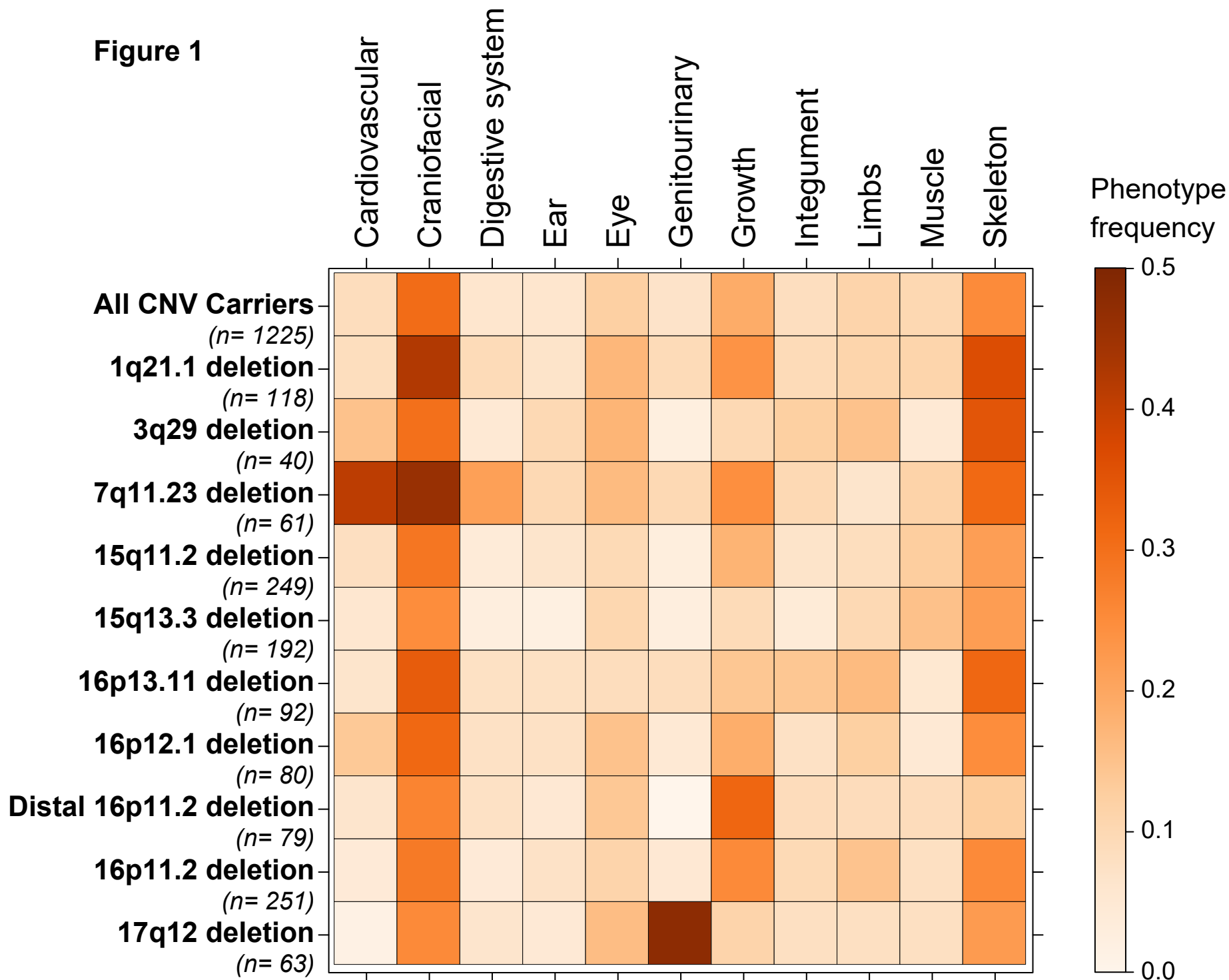
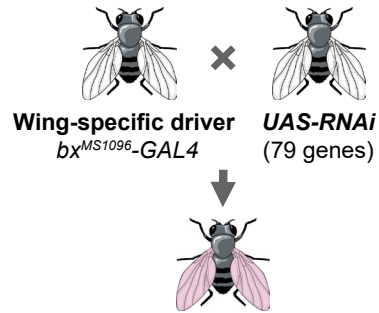


Figure 2

A Experimental strategy



Qualitative analysis

- Wrinkled wings
- Ectopic veins
- Missing veins
- Discoloration
- Bristle planar polarity

Quantitative analysis

- Longitudinal veins (L2,L3,L4,L5)
- Crossveins (ACV, PCV)
- Wing area

Tissue-specific effects

- Compare to ubiquitous knockdown
- Compare to eye-specific knockdown
- Gene expression across multiple tissues (Human and flies)

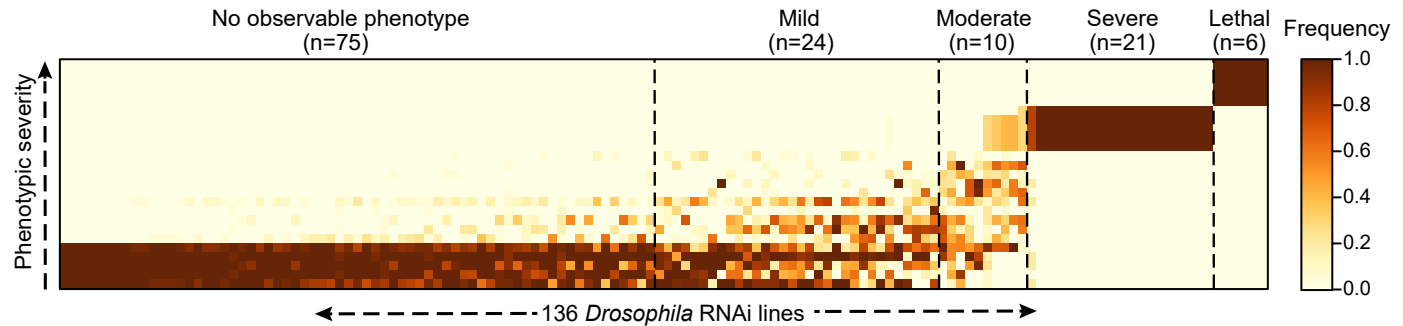
Cellular processes and developmental pathways

- Apoptosis
- Cell proliferation
- Disruptions in signaling pathways
- Human tissue-specific network analysis (Brain, heart, kidney)

B Phenotypic analysis of adult wings in *Drosophila*



C K-means clustering of qualitative wing data



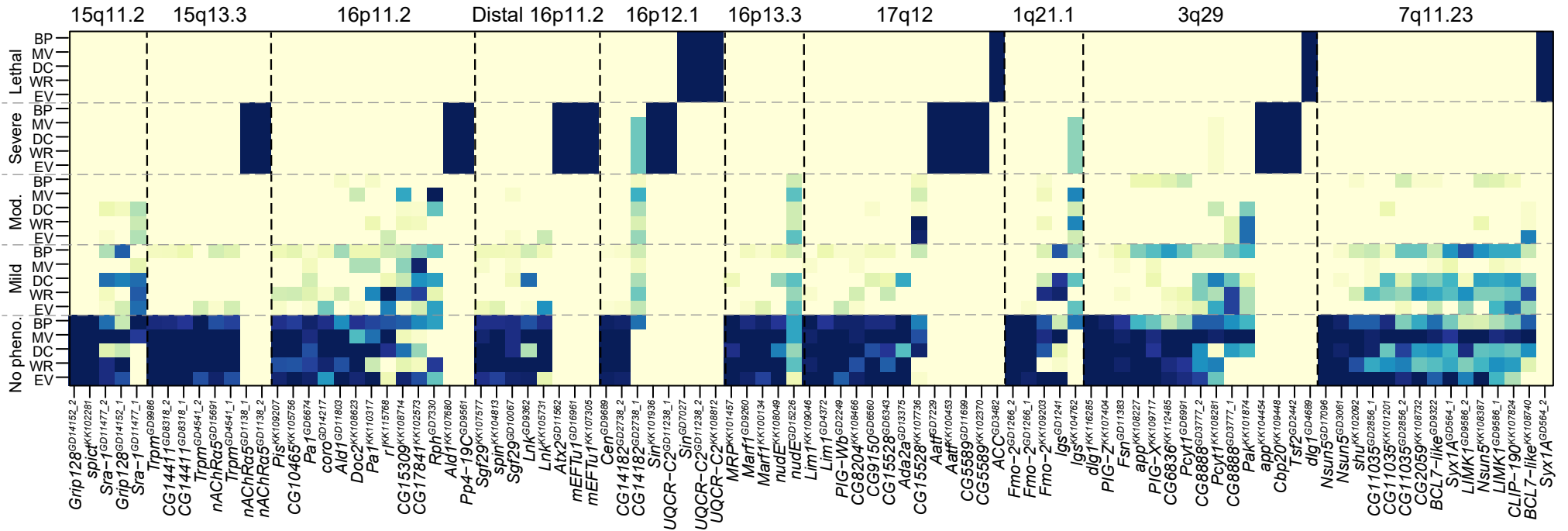
D Summary of qualitative and quantitative adult wing phenotypes

Fly homologs	RNAi lines	Qualitative phenotypes					Quantitative phenotypes	
		No pheno.	Mild	Moderate	Severe	Lethal	Wing area	L3 vein length
CNV genes (15q11.2, 15q13.3, 16p11.2, Distal 16p11.2, 16p12.1, 16p13.11, 17q12, 1q21.1, 3q29, 7q11.23)	95	45	21	7	16	6	65	53
Known neurodevelopmental genes (β -catenin, core genes, microcephaly)	41	30	3	3	5	0	24	21
Total	136	75	24	10	21	6	89	74

Figure 3

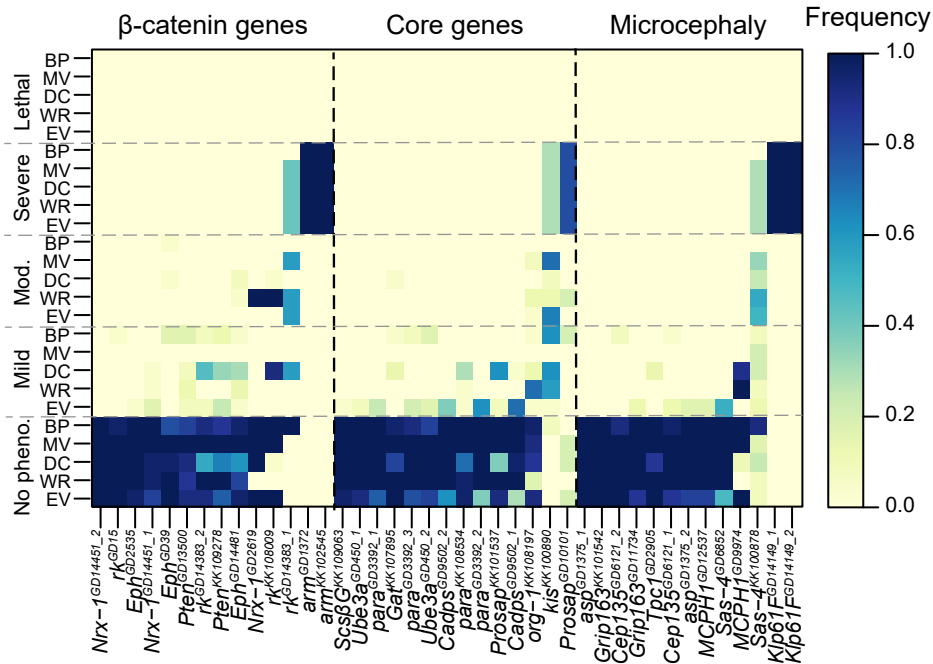
A

Qualitative wing phenotypes of homologs of CNV genes



B

Qualitative wing phenotypes of homologs of neurodevelopmental genes



C

Representative qualitative phenotypes in the adult wing

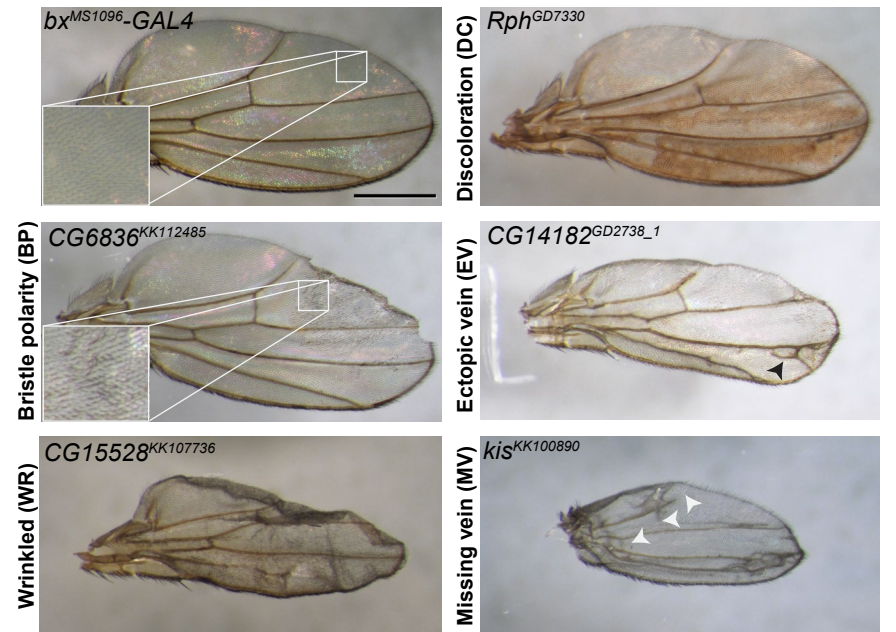
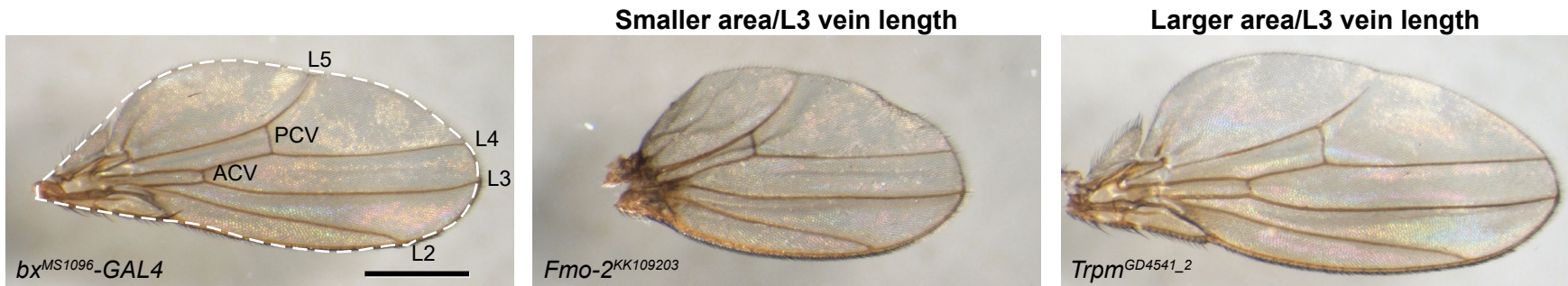
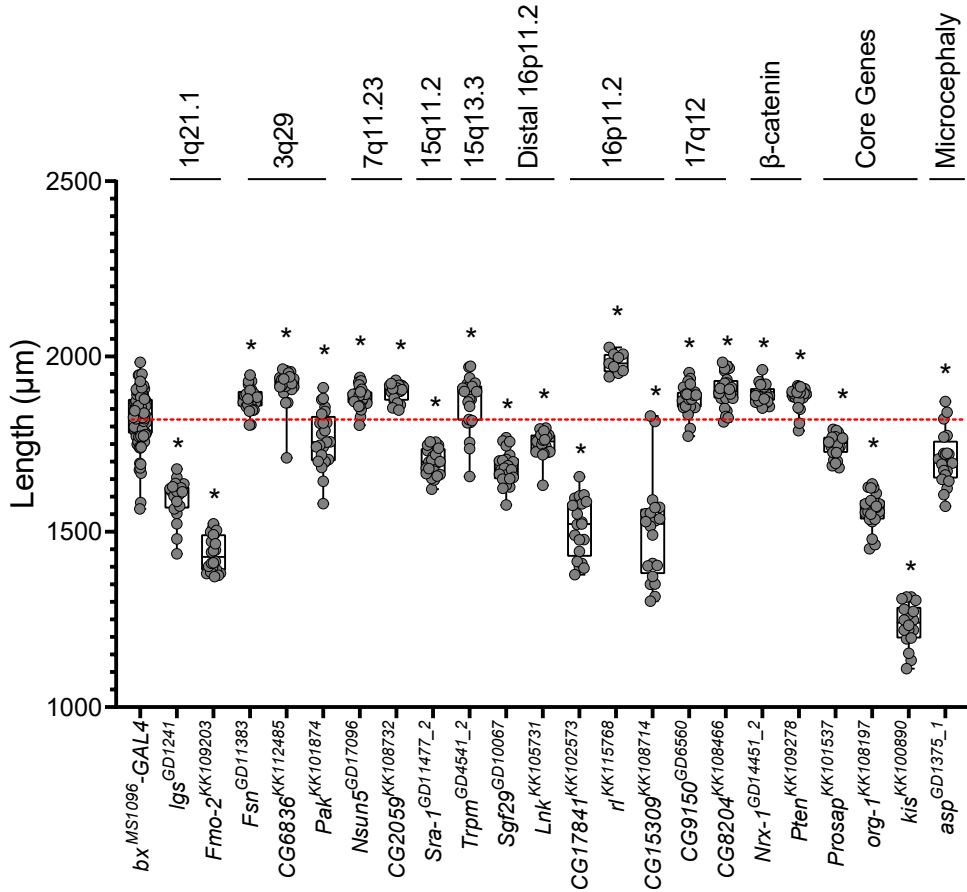


Figure 4

A Representative quantitative phenotypes in the adult wing



B L3 vein lengths for select homologs



C Wing area for select homologs

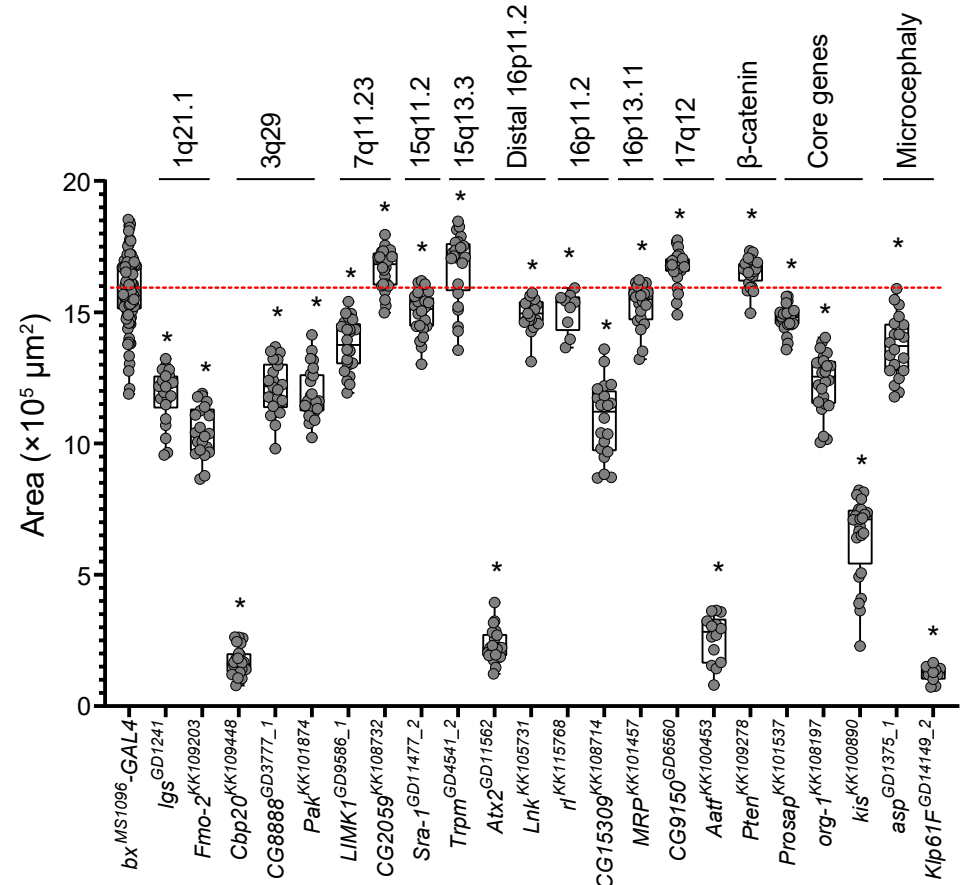
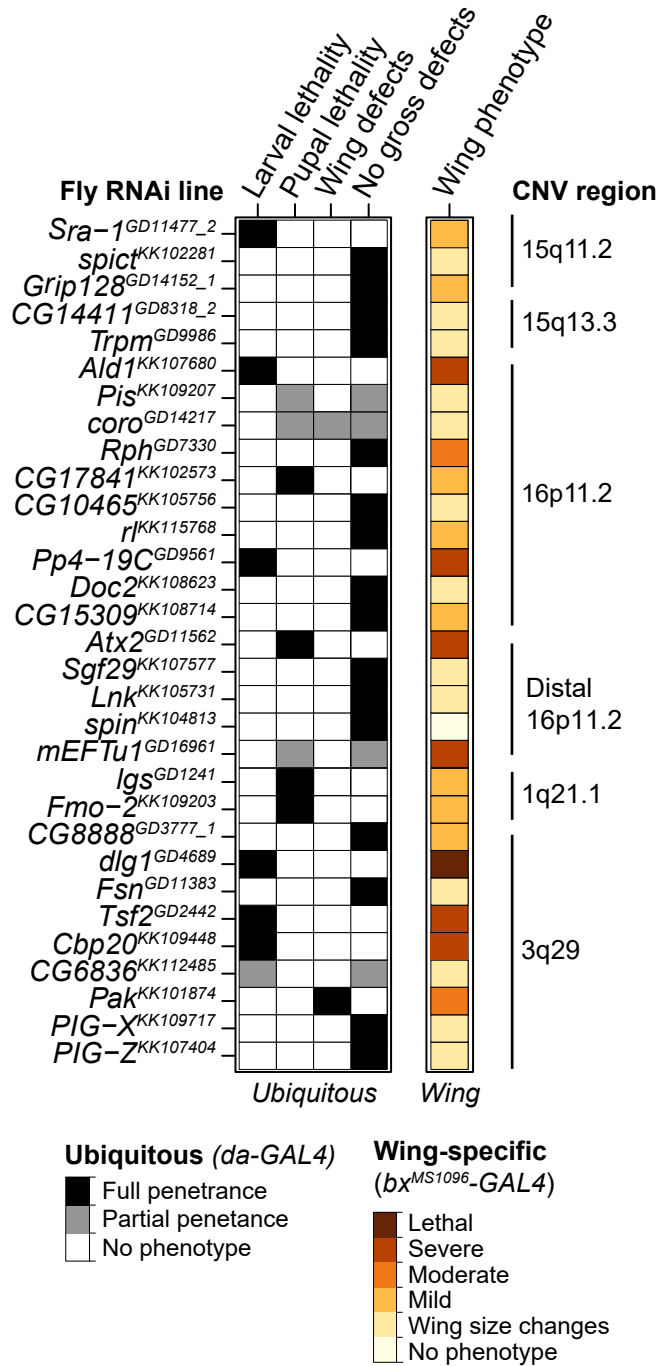
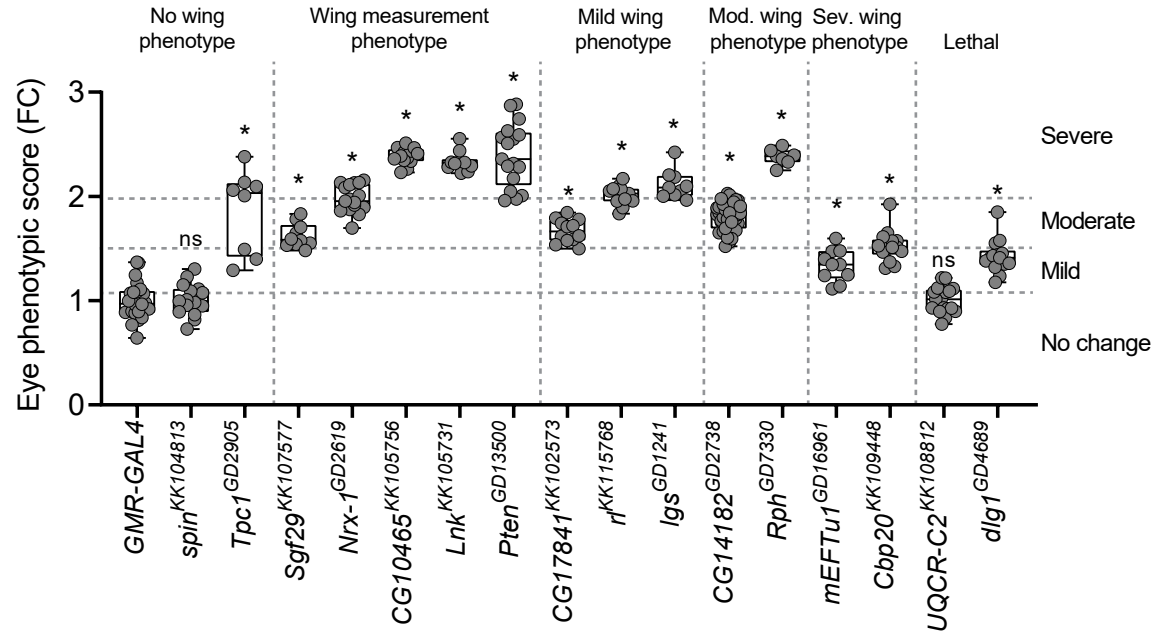


Figure 5

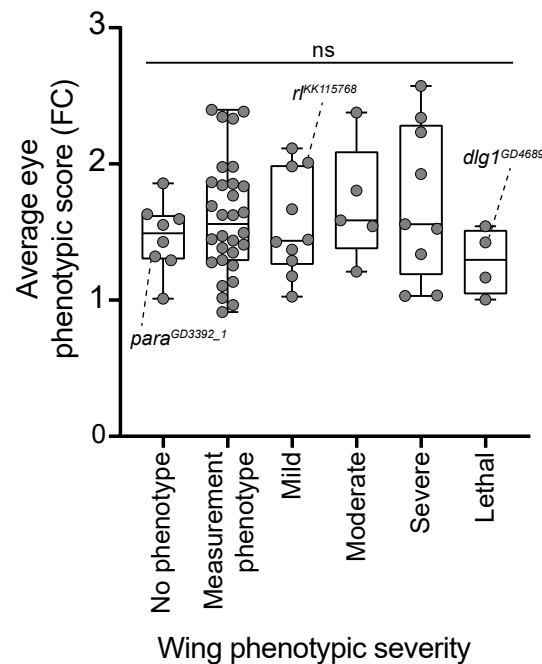
A Ubiquitous knockdown



B Eye versus wing phenotypes



C Severity of eye versus wing phenotype



D Representative eye and wing images

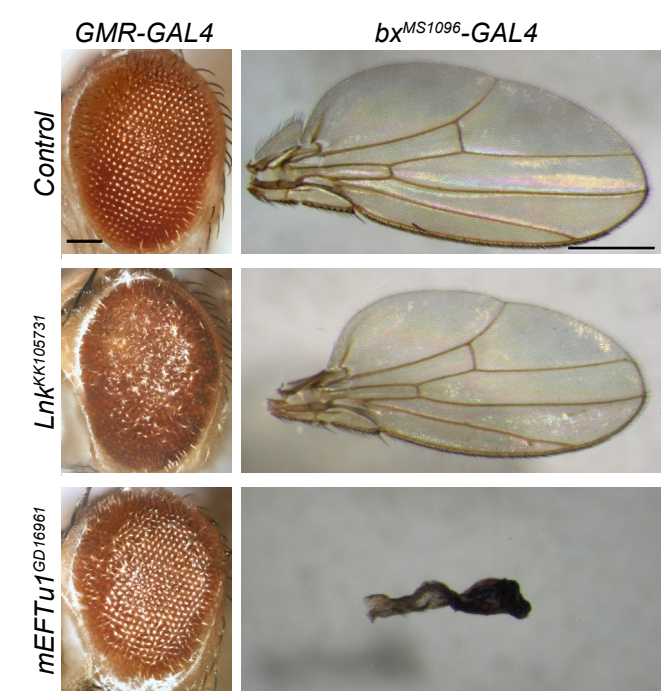
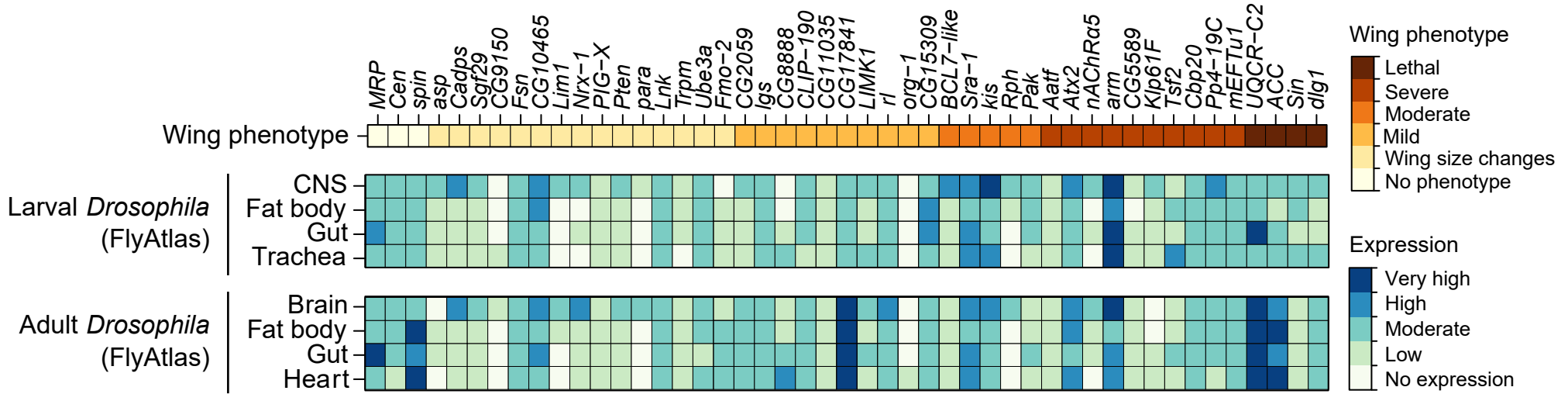


Figure 6

A Expression patterns of fly homologs of CNV genes across multiple fly tissues



B Expression patterns of CNV genes across multiple human tissues

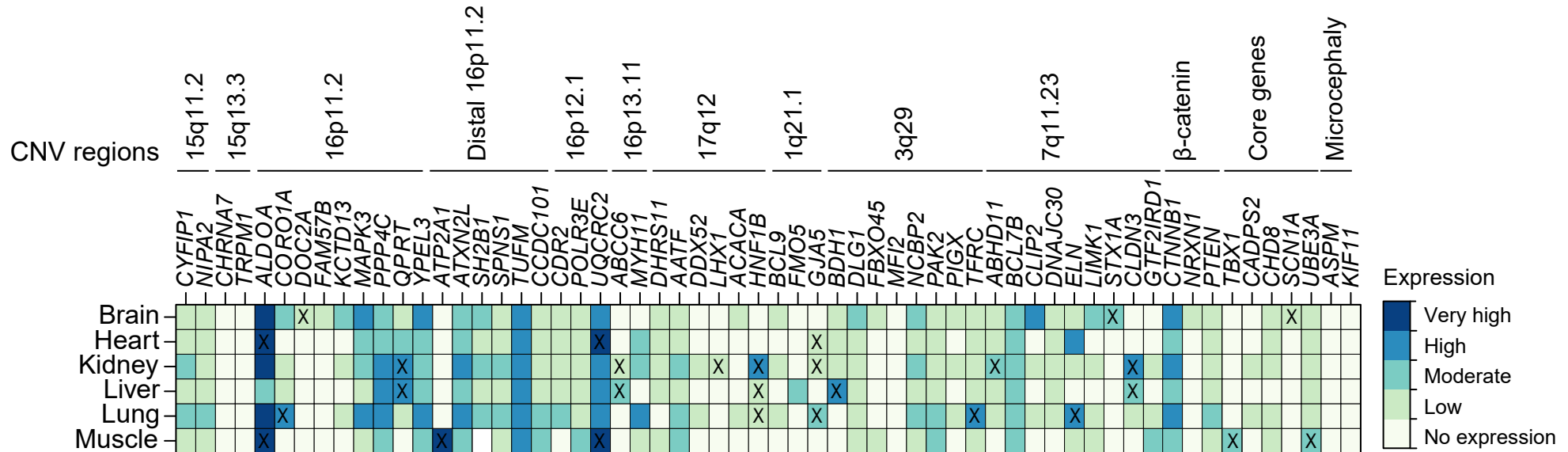
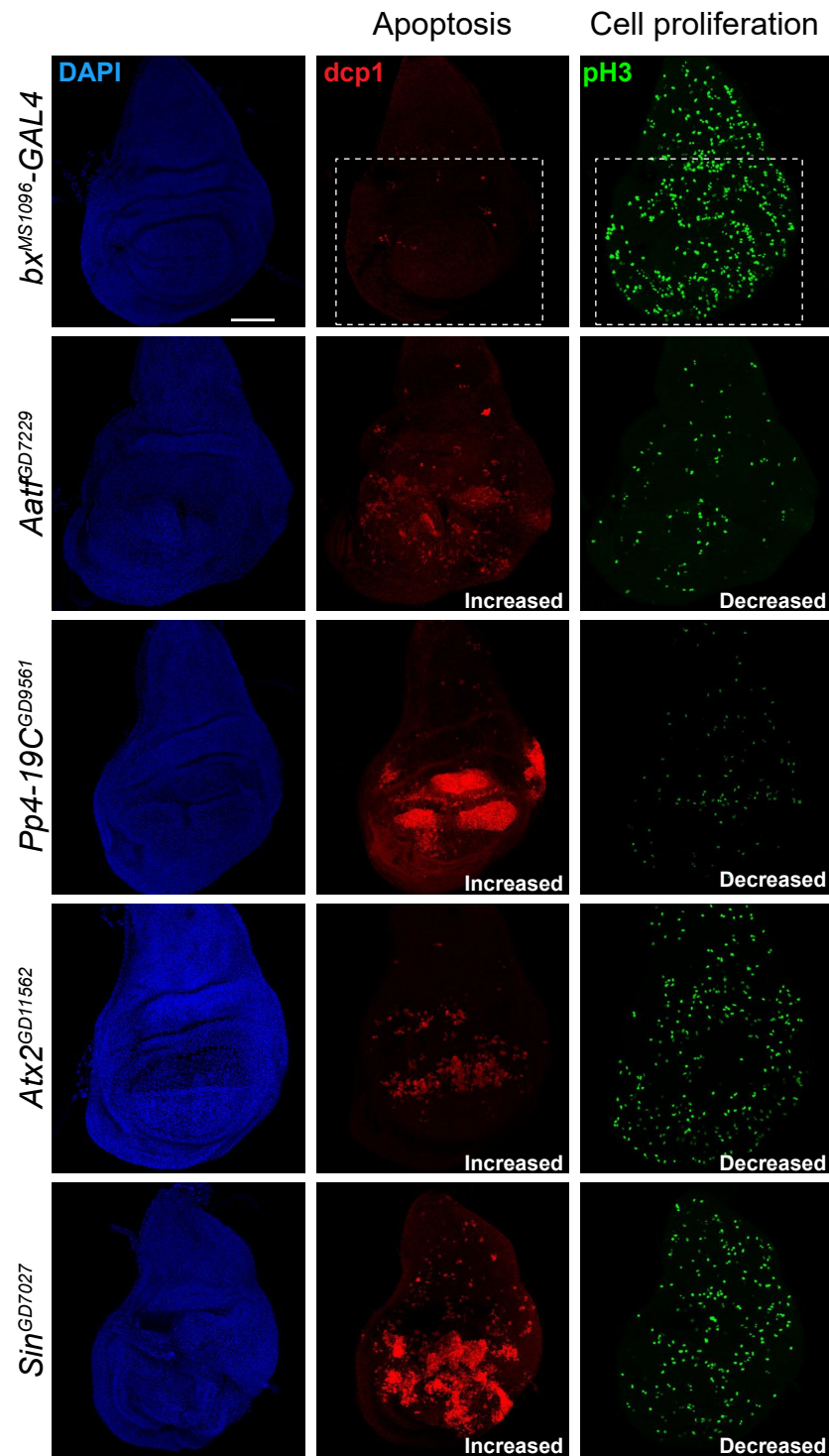
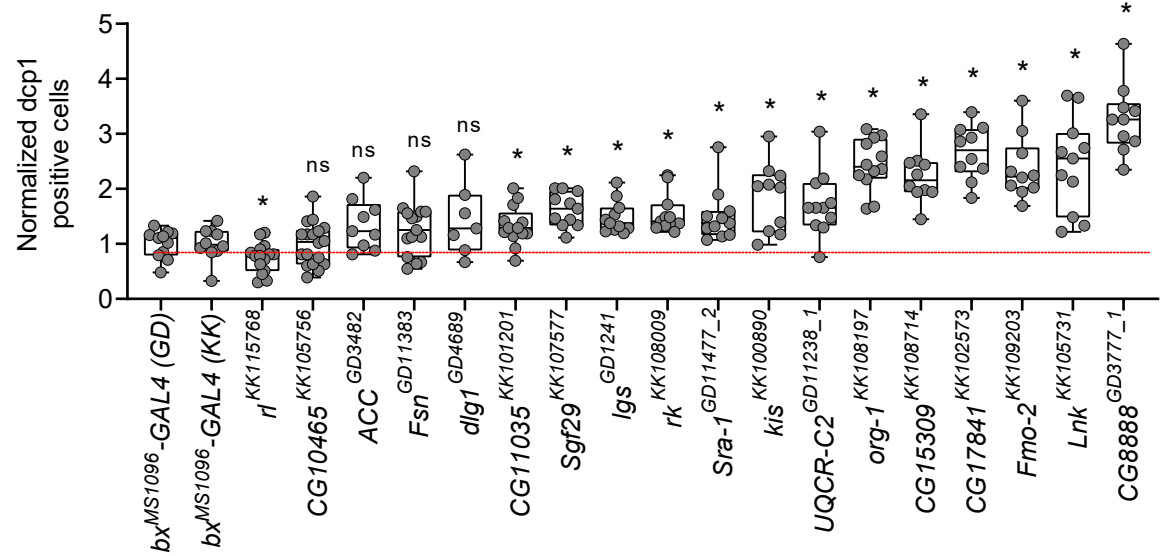


Figure 7

A Cellular processes in larval wing discs



B Quantification of apoptotic cells



C Quantification of proliferating cells

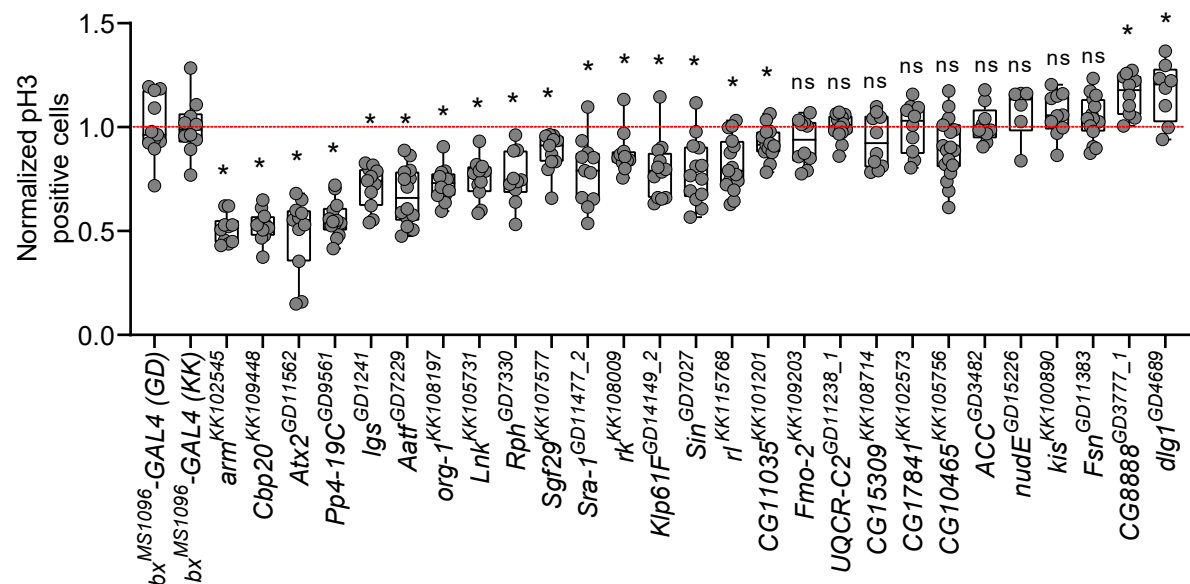


Figure 8

Disruption of signaling pathways in larval wing discs

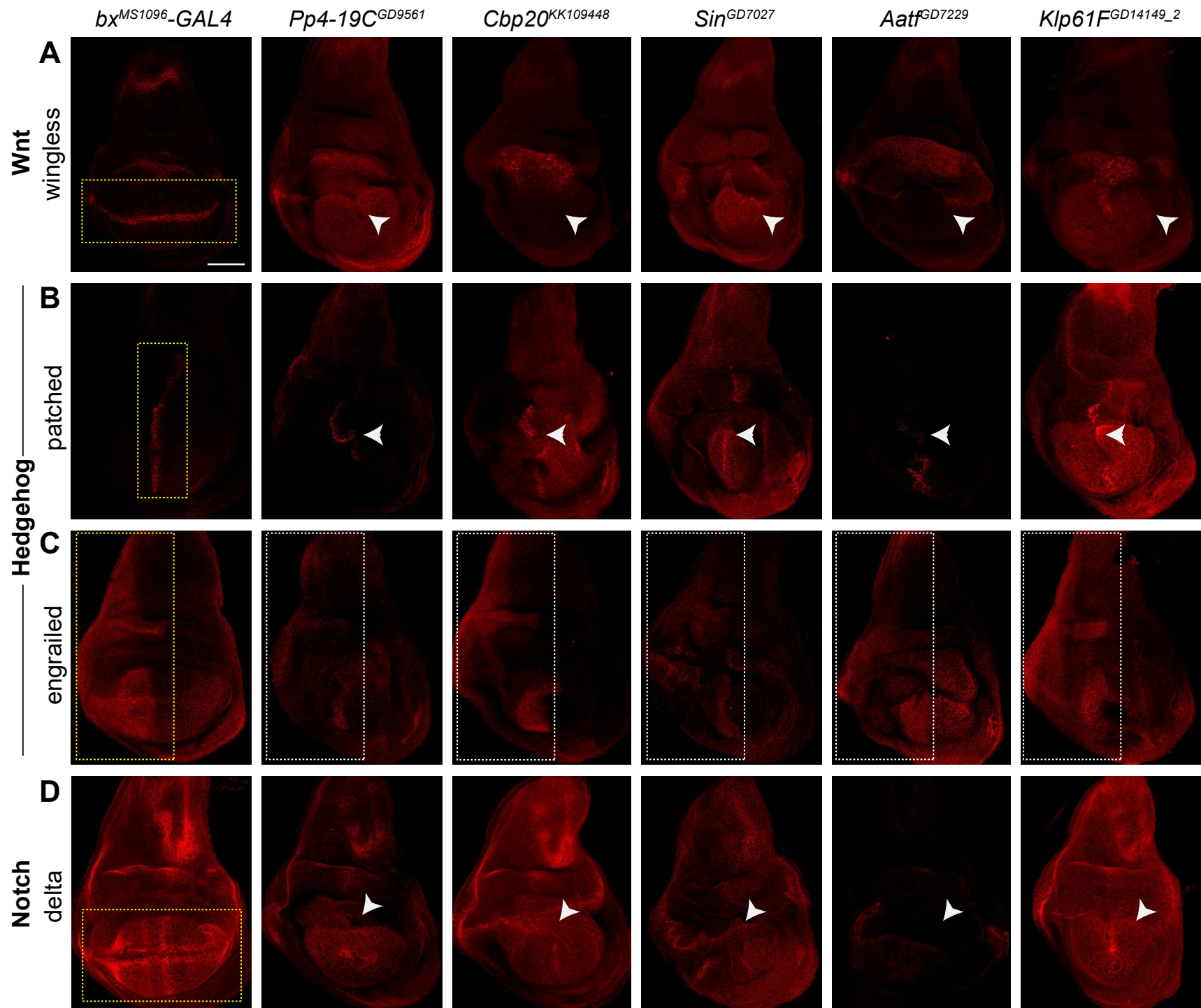


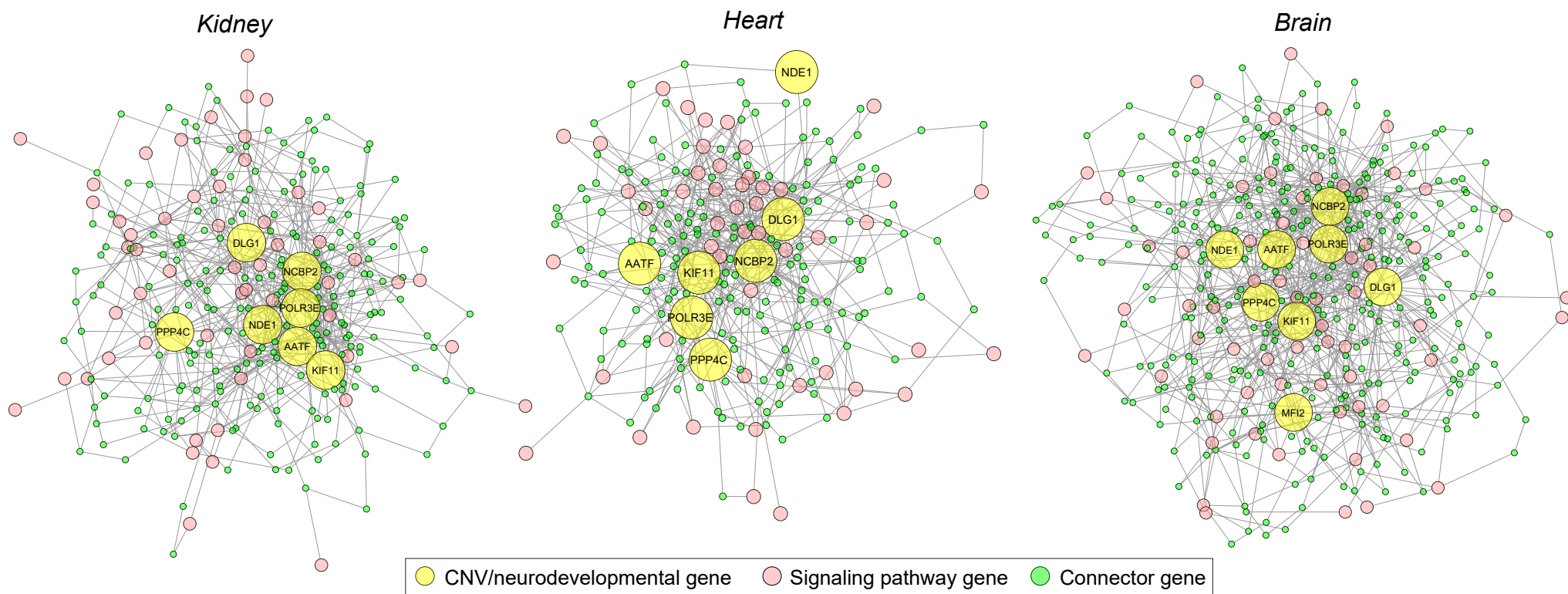
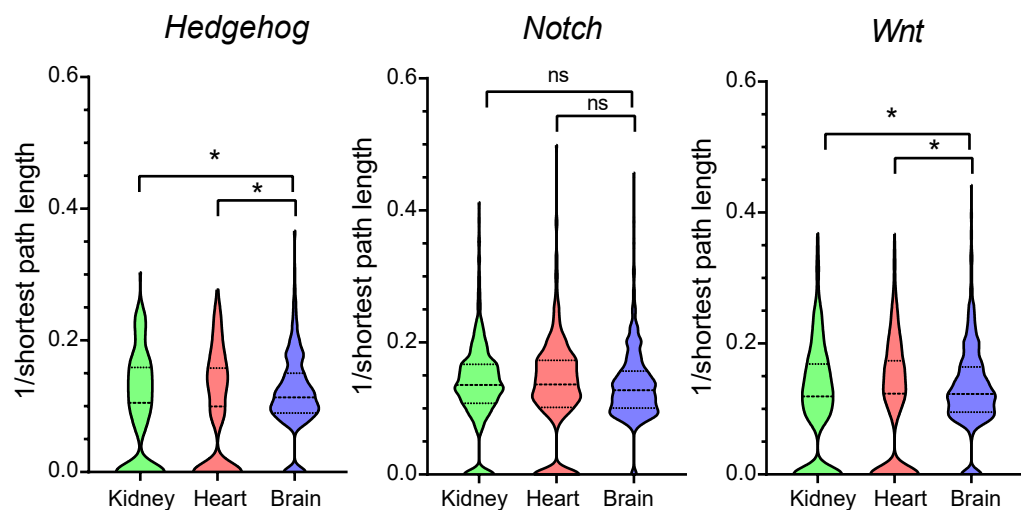
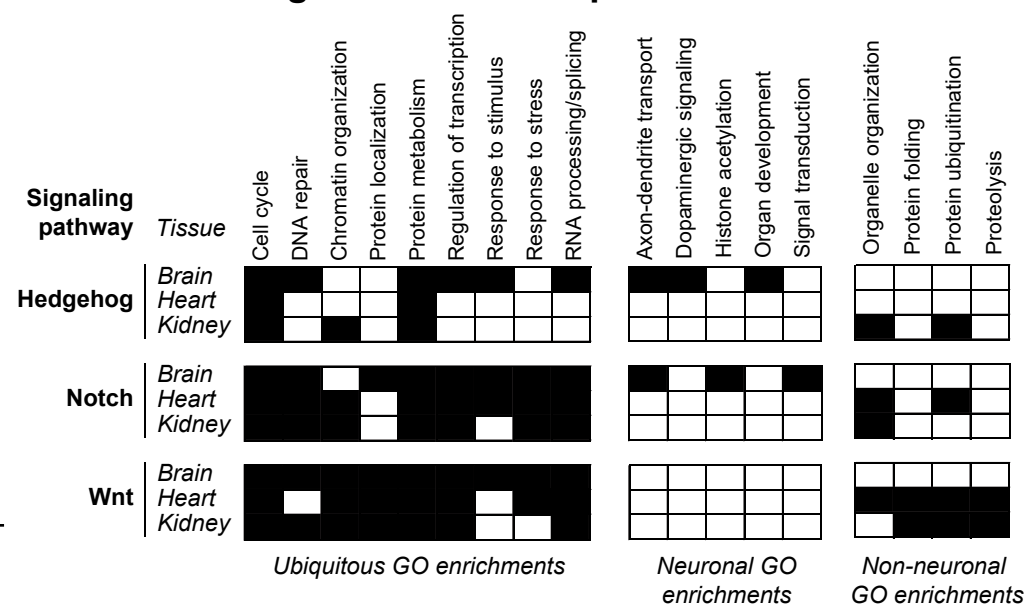
Figure 9**A Human CNV genes interact with Notch signaling pathway genes in multiple tissues****B Average connectivity of CNV genes to genes in signaling pathways****C GO term enrichment for connector genes in tissue-specific networks**

Figure 10

CNV region

